COMPARATIVE ASSESSMENT OF SECOND CANCER RISKS AFTER PROSTATE CANCER TREATMENT BY STEREOTACTIC BODY RADIOTHERAPY AND THREE-DIMENSIONAL CONFORMAL RADIOTHERAPY

RATTANA WATJIRANON

A THESIS SUBMITTED IN PARTIAL FULFILLMENT
OF THE REQUIREMENTS FOR
THE DEGREE OF MASTER OF SCIENCE (MEDICAL PHYSICS)
FACULTY OF GRADUATE STUDIES
MAHIDOL UNIVERSITY
2014

Thesis
entitled

COMPARATIVE ASSESSMENT OF SECOND CANCER RISKS AFTER PROSTATE CANCER TREATMENT BY STEREOTACTIC BODY RADIOTHERAPY AND THREE-DIMENSIONAL CONFORMAL RADIOTHERAPY

Rattana Watjiranon
.....
Miss Rattana Watjiranon
Candidate

.....
Assoc. Prof. Vipa Boonkitticharoen,
Ph.D. (Radiation Biology)
Major advisor

Chomporn Sitathanee
.....
Asst. Prof. Chomporn Sitathanee,
M.D.
Co-advisor

Mantana Dhanachai
.....
Assoc. Prof. Mantana Dhanachai,
M.D., M.Sc. (Medical Epidemiology)
Co-advisor

B. Mahaisavariya
.....
Prof. Banchong Mahaisavariya,
M.D., Dip. Thai Board of Orthopedics
Dean
Faculty of Graduate Studies
Mahidol University

Puangpen Tangboonduangjit
.....
Lect. Puangpen Tangboonduangjit,
Ph.D. (Medical Radiation Physics)
Program Director
Master of Science Program
in Medical Physics
Faculty of Medicine
Ramathibodi Hospital
Mahidol University

Thesis
entitled

COMPARATIVE ASSESSMENT OF SECOND CANCER RISKS AFTER PROSTATE CANCER TREATMENT BY STEREOTACTIC BODY RADIOTHERAPY AND THREE-DIMENSIONAL CONFORMAL RADIOTHERAPY

was submitted to the Faculty of Graduate Studies, Mahidol University
for the degree of Master of Science (Medical Physics)
on
March 21, 2014

Rattana Watjiranon
.....
Miss Rattana Watjiranon
Candidate

.....
Assoc. Prof. Kanjana Shotelersuk, M.D.
Chair

.....
Assoc. Prof. Vipa Boonkitticharoen, Ph.D. (Radiation Biology)
Member

Chomporn Sitathanee
.....
Asst. Prof. Chomporn Sitathanee, M.D.
Member

Mantana Dhanachai
.....
Assoc. Prof. Mantana Dhanachai, M.D., M.Sc. (Medical Epidemiology)
Member

B. Mahaisavariya
.....
Prof. Banchong Mahaisavariya, M.D., Dip. Thai Board of Orthopedics
Dean
Faculty of Graduate Studies
Mahidol University

.....
Prof. Winit Phuapradit, M.D., M.P.H.
Dean
Faculty of Medicine
Ramathibodi Hospital,
Mahidol University

ACKNOWLEDGEMENTS

I would like to express my sincere gratitude and deep appreciation to my major advisor, Assoc. Prof. Vipa Boonkitticharoen for her valuable advice, guidance, supervision, encouragement and assistance throughout this thesis. In addition, I am equally grateful to Asst. Prof. Chomporn Sitathanee and Assoc. Prof. Mantana Dhanachai my co-advisor for their important suggestions and comments in this experiment.

I would also like to express my appreciation to Mrs. Pornpan Yongvithisatid, Miss. Patchareporn Dechsupa and Miss Kumutinee Pairat for their training of the use the computerized treatment planning system (MultiPlan®) and advices about performance of CyberKnife. I also express my appreciation to Miss Pimolpun Changkaew and Miss Siwaporn Sakulsingharoj for their training of the use the computerized treatment planning system (Eclipse 8.9.15) and the helpful advice on thermoluminescence dosimeter. Specially thanks is express to Miss Supaporn Srisuwan and Mr. Thawesak Ukamphan for their assistance with the collection of my data.

I am particularly grateful for kindness in examining the research and providing suggestions for improvement given by Assoc. Prof. Kanjana Shotelersuk.

I wish to thank all teachers, lecturers, staffs and my classmates in the School of Medical Physics, Mahidol University for their kind support and teaching me in the Medical Physics Program.

Finally, I have to sincerely regard mention to my parents. Thank you for their understanding and inspiration throughout my whole study. The usefulness of this thesis, I dedicate to my family and all teachers who have taught me since my childhood.

Rattana Watjiranon

COMPARATIVE ASSESSMENT OF SECOND CANCER RISKS AFTER PROSTATE CANCER TREATMENT BY STEREOTACTIC BODY RADIOTHERAPY AND THREE-DIMENSIONAL CONFORMAL RADIOTHERAPY

RATTANA WATJIRANON 5236469 RAMP/M

M.Sc. (MEDICAL PHYSICS)

THESIS ADVISORY COMMITTEE: VIPA BOONKITTICHAROEN, Ph.D. (RADIATION BIOLOGY), CHOMPORN SITATHANEE, M.D., MANTANA DHANACHAI, M.D., M.Sc. (MEDICAL EPIDEMIOLOGY)

ABSTRACT

The purpose of this study assessed the second cancer risks in in-field (planning target volume, PTV) and organs at beam border (bladder and rectum) in patients with prostate cancer treated by CyberKnife stereotactic body radiotherapy (CK-SBRT) compared to three-dimensional conformal radiotherapy (3D-CRT). The risk of second cancer was determined based on the organ equivalent dose (OED) formulated by Schneider et al. The OED estimate was the summation of OED from primary beam, scatter/leakage and imaging dose. Treatment plans for six patients were optimized using MultiPlan® treatment planning system (TPS) of CK-SBRT and Eclipse TPS (Version 8.9.15) of 3D-CRT. Six MV photons were delivered according to CK-SBRT plan in 5 fractions of 7.25 Gy and 10 MV photons for 3D-CRT plan in 38 fractions of 2 Gy. OED for primary beam was calculated from the differential dose volume histogram (dDVH) while scatter/leakage radiation and imaging dose for each treatment plan were measured in Rando phantom by thermoluminescence dosimeter.

For PTV, the total OED generated by CK-SBRT was 1.4 times less than that of 3D-CRT ($p << 0.0001$). In contrast, bladder OED by CK-SBRT was significantly greater than that of 3D-CRT ($p = 0.0005$). For rectum, greater scatter/leakage OED ($p = 0.036$) observed for CK-SBRT was compensated by lower image OED ($p = 0.0004$) to render nearly equal total OED for both techniques. Overall, the primary OED contributed > 95% to total OED, followed by image OED (between 1 - 4% contributions) and scatter/leakage OED (< 1% contribution). The magnitude of total OED is mainly governed by primary beam targeting. CK-SBRT generates greater scatter/leakage OED than 3D-CRT but the risk is extremely small.

KEY WORDS: SECOND CANCERS / SBRT / 3D-CRT / ORGAN EQUIVALENT DOSE

68 pages.

การเปรียบเทียบความเสี่ยงต่อมะเร็งทุติยภูมิในผู้ป่วยมะเร็งต่อมลูกหมากจากการบำบัดโดยรังสีรักษาร่วมพิกัดแบบทั่วร่างกายและรังสีรักษาสามมิติ

COMPARATIVE ASSESSMENT OF SECOND CANCER RISKS AFTER PROSTATE CANCER TREATMENT BY STEREOTACTIC BODY RADIOTHERAPY AND THREE-DIMENSIONAL CONFORMAL RADIOTHERAPY

รัตนา วัฒน์จิรานนท์ 5236469 RAMP/M

วท.ม. (ฟิสิกส์การแพทย์)

คณะกรรมการที่ปรึกษาวิทยานิพนธ์: วิภา บุญกิตติเจริญ, Ph.D. (RADIATION BIOLOGY),
ชมพร สีตะธนี, M.D., มัณฑนา ธนะไชย, M.D., M.Sc. (MEDICAL EPIDEMIOLOGY)

บทคัดย่อ

วัตถุประสงค์ของงานวิจัยนี้คือการประเมินความเสี่ยงต่อการเกิดมะเร็งทุติยภูมิในปริมาตรของรังสีบำบัดและอวัยวะที่ติดกับขอบลำรังสี (กระเพาะปัสสาวะและลำไส้ตรง) ในผู้ป่วยมะเร็งต่อมลูกหมากจากการบำบัดด้วยรังสีรักษาร่วมพิกัดแบบทั่วร่างกายด้วยเครื่อง CyberKnife (CK-SBRT) เปรียบเทียบกับรังสีรักษาสามมิติ (3D-CRT) ความเสี่ยงต่อมะเร็งทุติยภูมิวัดจาก organ equivalent dose (OED) ที่เสนอโดย Schneider และคณะ ซึ่งการประเมินด้วย OED ได้จากผลรวมของ OED จากรังสีปฐมภูมิ รังสีกระเจิง/รังสีรั่วไหลและรังสีการถ่ายภาพ จากการวางแผนการรักษาที่เหมาะสมในผู้ป่วยมะเร็งต่อมลูกหมากจำนวน 6 ราย ด้วยเครื่องคอมพิวเตอร์วางแผนการรักษา MultiPlan® สำหรับ CK-SBRT และเครื่องวางแผนการรักษา Eclipse 8.9.15 สำหรับ 3D-CRT ที่พลังงาน 6 MV จำนวน 5 ครั้ง ครั้งละ 7.25 Gy สำหรับการบำบัดด้วยวิธี CK-SBRT และจำนวน 38 ครั้ง ครั้งละ 2 Gy ตามแผนการบำบัดด้วยวิธี 3D-CRT โดย OED ของรังสีปฐมภูมิคำนวณจาก differential dose volume histogram (dDVH) ในขณะที่ OED ของรังสีกระเจิง/รังสีรั่วไหลและรังสีการถ่ายภาพในแต่ละแผนการรักษาได้จากการวัดภายใน Rando phantom โดยใช้ thermoluminescence dosimeter

OED ในปริมาตรของรังสีบำบัดด้วยวิธี CK-SBRT มีค่าน้อยกว่า 3D-CRT ประมาณ 1.4 เท่า ($p << 0.0001$) ในทางตรงข้ามค่า OED ในกระเพาะปัสสาวะจากการบำบัดด้วยวิธี CK-SBRT มีค่าสูงกว่าค่า OED จากการบำบัดด้วย 3D-CRT ($p = 0.0005$) สำหรับลำไส้ตรง OED ของรังสีกระเจิง/รังสีรั่วไหลจากการบำบัดด้วย CK-SBRT มีค่าสูงกว่าเมื่อเทียบกับ 3D-CRT ($p = 0.036$) แต่ถูกหักล้างด้วย OED ของรังสีการถ่ายภาพที่น้อยกว่า 3D-CRT ($p = 0.0004$) จึงทำให้ OED รวมจากวิธี CK-SBRT มีค่าใกล้เคียงกับ OED รวมจากวิธี 3D-CRT โดยมากกว่า 95% ของ OED รวมจากวิธี CK-SBRT และ 3D-CRT เป็นผลมาจาก OED ของรังสีปฐมภูมิ ตามด้วย OED ของรังสีการถ่ายภาพ (ประมาณ 1 - 4%) และ OED ของรังสีกระเจิง/รังสีรั่วไหล (น้อยกว่า 1%) ดังนั้นปริมาณของ OED รวมส่วนใหญ่จะเป็นผลมาจากรังสีปฐมภูมิ สำหรับการบำบัดด้วยวิธี CK-SBRT แม้ว่าจะมีค่า OED ของรังสีกระเจิง/รังสีรั่วไหลสูงกว่าวิธี 3D-CRT แต่ความเสี่ยงที่เป็นผลจากรังสีกระเจิง/รังสีรั่วไหลมีค่าน้อยมาก

68 หน้า

CONTENTS

		Page
ACKNOWLEDGEMENTS		iii
ABSTRACT (ENGLISH)		iv
ABSTRACT (THAI)		v
LIST OF TABLES		vii
LIST OF FIGURES		ix
LIST OF ABBREVIATIONS		x
CHAPTER I	INTRODUCTION	1
CHAPTER II	OBJECTIVES	4
CHAPTER III	LITERATURE REVIEWS	5
CHAPTER IV	MATERIALS AND METHODS	10
CHAPTER V	RESULTS	25
CHAPTER VI	DISCUSSION	46
CHAPTER VII	CONCLUSIONS	50
REFERENCES		51
APPENDIX		56
BIOGRAPHY		68

LIST OF TABLES

Table		Page
4.1	The CK-SBRT treatment plans for six patients with prostate cancer.	17
4.2	The 3D-CRT treatment plans for six patients with prostate cancer.	18
4.3	Points of measurement for scatter/leakage dose in Rando phantom.	21
4.4	Points of measurement for image dose in the Rando phantom.	23
5.1	EQD_2 for PTV treated by CK-SBRT and 3D-CRT.	25
5.2	EQD_2 for bladder treated by CK-SBRT and 3D-CRT.	26
5.3	EQD_2 for rectum treated by CK-SBRT and 3D-CRT.	26
5.4	OED_{prim} for PTV treated by CK-SBRT and 3D-CRT.	27
5.5	OED_{prim} for bladder treated by CK-SBRT and 3D-CRT.	27
5.6	OED_{prim} for rectum treated by CK-SBRT and 3D-CRT.	28
5.7	Comparison between OED_{prim}'s from CK-SBRT and 3D-CRT.	28
5.8	Scatter/leakage dose (Gy/MU) from TLD measurement in 10 positions outside the treatment field from CK-SBRT and 3D-CRT.	30
5.9	Scatter/leakage dose (D_{SL}) to organ outside the treatment field at 10 positions from CK-SBRT and 3D-CRT.	31
5.10	Whole body scatter/leakage doses (D_{SL}) from CK-SBRT and 3D-CRT.	32
5.11	PTV $OED_{scatter/leakage}$ for CK-SBRT and 3D-CRT plans.	33
5.12	Bladder $OED_{scatter/leakage}$ for CK-SBRT and 3D-CRT plans.	33
5.13	Rectum $OED_{scatter/leakage}$ for CK-SBRT and 3D-CRT plans.	34
5.14	Comparison between $OED_{scatter/leakage}$'s from CK-SBRT and 3D-CRT.	34
5.15	Image doses from 150 exposures in 15 positions for CK-SBRT technique with exposure technique set at 120 kV, 10 mAs. Data are means (SD).	35
5.16	Imaging doses estimated for PTV, bladder and rectum in CK-SBRT treatment.	36

LIST OF TABLES (cont.)

Table		Page
5.17	Image doses from field and setup verification for 3D-CRT technique measured in 15 positions with 6 MV photon beam. Data are means (SD).	37
5.18	Image doses (Gy) from field and setup verification for 3D-CRT technique with 6 MV photon beam. Data are means (SD).	38
5.19	OED_{image} for CK-SBRT and 3D-CRT.	39
5.20	OED_T for PTV from CK-SBRT and 3D-CRT.	41
5.21	OED_T for bladder from CK-SBRT and 3D-CRT.	42
5.22	OED_T for rectum from CK-SBRT and 3D-CRT.	43
5.23	Comparison between OED_T's from CK-SBRT and 3D-CRT.	44
A.1	The element correction coefficient (ECC_i) value for TLD-700.	59
A.2	The individual element correction coefficient (ECC_{ci}) for TLD-700.	61
A.3	The element correction coefficient (ECC_i) value for TLD-100H.	65
A.4	The individual element correction coefficient (ECC_{ci}) for TLD-100H.	66

LIST OF FIGURES

Figure		Page
3.1	The dose-response curve for radiation induced thyroid cancer.	7
3.2	The dose-response curve for radiation induced cancer of breast, bladder and stomach after radiotherapy.	7
4.1	Accuray CyberKnife G4 system.	11
4.2	Varian Clinac iX linear accelerator.	12
4.3	The Alderson Rando phantom.	13
4.4	Array of thermoluminescence dosimeter (TLD-700) in the TLD planchet.	14
4.5	Array of thermoluminescence dosimeter (TLD-100H) in the TLD planchet.	14
4.6	The automatic TLD reading system.	15
4.7	The TLD annealing oven.	16
4.8	Positions of TLD in Rando phantom for the scatter/leakage dose measurement.	22
4.9	Positions of TLD in Rando phantom for the image dose measurement.	24
5.1	The average OEDs for primary beam, scatter/leakage radiation, imaging and total OED for PTV from CK-SBRT and 3D-CRT.	44
5.2	The average OEDs for primary beam, scatter/leakage radiation, imaging and total OED for bladder from CK-SBRT and 3D-CRT.	45
5.3	The average OEDs for primary beam, scatter/leakage radiation, imaging and total OED for rectum from CK-SBRT and 3D-CRT.	45
A.1	The linearity of TLD-700.	63
A.2	The linearity of TLD-100H.	67

LIST OF ABBREVIATIONS

Abbreviation	Term
3D-CRT	Three-dimensional conformal radiotherapy
B_w	Backscatter factor
cm	Centimeter
cm^2	Square centimeter
cm^3	Cubic centimeter
C	Coulomb
CK-SBRT	Stereotactic body radiotherapy using CyberKnife
CT	Computed tomography
Cu	Copper
^oC	Degree Celsius
dDVH	Differential dose volume histogram
d_i	Dose per fraction
D_i	Dose
D_{SL}	Scatter and leakage dose
D_u	Unknown dose
DVH	dose volume histogram
ECC_{ci}	Individual element correction coefficient
ECC_i	Element correction coefficient
EPID	Electronic portal imaging device
EQD_2	Biologically equivalent dose in 2 Gy/fraction
g	Gram
G	Body density
GTV	Gross tumor volume
Gy	Gray
HVL	Half value layer
kg	Kilogram

LIST OF ABBREVIATIONS (cont.)

Abbreviation	Term
kV	Kilovoltage
Li	Lithium
LiF	Lithium fluoride
Lt	Left side
m	Meter
mA	Milli-ampere
mAs	Milli-ampere second
MeV	Megaelectron volt
Mg	Magnesium
mm	Millimeter
MRI	Magnetic Resonance Imaging
ms	Millisecond
MU	Monitor unit
MV	Megavolt
nC	Nanocoulomb
OED	Organ equivalent dose
OED_{image}	Organ equivalent dose for image dose
OED_{prim}	Organ equivalent dose for primary beam
$OED_{scatter/leakage}$	Organ equivalent dose for scatter and leakage radiation
OED_T	Total organ equivalent dose
P	Phosphorus
PTV	Planning target volume
Q_{ci}	Corrected charge integral
Q_i	individual reading of each TLD
RCF	Reader calibration factor
RISM	Radiation-induced secondary malignancies
Rt	Right side

LIST OF ABBREVIATIONS (cont.)

Abbreviation	Term
SBRT	Stereotactic body radiotherapy
SD	Standard deviation
Ti	Titanium
TLD	Thermoluminescence dosimeter
V_{WB}	Volume of whole body
WB	Whole body weight
α	A model parameter describing cell killing
β	A model parameter describing cell repopulation

CHAPTER I
INTRODUCTION

Prostate cancer (PCa) is the second most common cancer and the sixth leading cause of cancer death among men worldwide [1]. PCa incidence rates vary markedly from <10 (per 100,000) in the Republic of Korea, Thailand and India to >100 in the United States and New Zealand [1]. But mortality rates tended to be higher in less developed nations. Type of PCa treatment and underlying risks including old age, ethnicity, and family history of the disease are factors affecting rates of PCa mortality and trends [1, 2]. The treatment for PCa usually includes surgery and radiotherapy. However, surgery may not be appropriate in all patients, particularly for older patients and those in whom the likelihood of organ-confined disease is lower. Radiotherapy is the treatment choice for such patients and is often used to treat all stages of PCa. In addition, radiotherapy is a non-invasive technique which may reduce the risk of complications after surgery [3].

The increasing trend toward the detection of PCa at a younger age and earlier stage [4] and the availability of successful treatment options serve the main driving forces in increasing long-term survivorship. In the last decade, radiotherapy (RT) proved to have an equal efficiency compared to surgery in treatment of PCa. Various techniques of RT including brachytherapy, proton beam therapy and conformal radiotherapy (CRT) are used in management of clinically localized PCa [5]. Increase in patient survival following RT has been accounted by a number of strategies including dose escalation, target volume definition and organ movement tracking [6]. Long-term patient survival raises the issue of radiation-induced secondary malignancies (RISM).

It has been well established that RISM is a late phenomenon with a long latent period which might be inversely related to radiation dose. A study on pelvic irradiation reported by Quilty and Kerr [7] revealed that mean latent periods of bladder cancer after low dose and high dose irradiation are 30 and 16.5 years, respectively.

However, RISM is generally defined as cancers which arise after a latency period around 10 years inside or close to the treatment volume [8]. Sometimes, a latency of at least 5 years is also acceptable [9]. Risks of RISM after prostate irradiation were reported by several single institution/registry and multiregistry (SEER, Surveillance, Epidemiology and End Results) epidemiological studies involving RT in the two-dimensional (2D) era [10]. Data of single institution/registry studies are more informative than the multiregistry series for the knowledge of doses and type of treatment technique but are less conclusive for the time being because of small number of patients and relatively short follow-up. Multiregistry studies although included large number of patients (range: 85,815-144,761) had certain deficiencies including limited data of risk factors, insufficient details of therapy. Despite these limitations, findings from multiregistry studies suggest a modest increase in RISM after prostate radiation as approximately one in 70 patients undergoing prostate radiation and surviving more than 10 years will develop secondary cancer. The most common sites of RISM are organs adjacent to the radiation field, i.e. bladder and rectum [10]. In-field sarcoma [11, 12] and lung cancer at distant site are also reported [12, 13]. The increase risk of RISM is observed for patients treated by conventional 2D-RT, not after brachytherapy [10]. Modern radiotherapeutic techniques such as intensity-modulated radiotherapy (IMRT), stereotactic body radiotherapy (SBRT) may be associated with a higher risk of secondary cancers for generating greater scatter/leakage radiation than conventional RT [14] and subjecting to concomitant dose exposure from image-guided localization and verification procedures [15].

Assessment of RISM can also be conducted by dosimetric study [15]. Since RT increases the risk of RISM in a dose-dependent manner and most secondary cancers developed within or at the edge of the radiation field [16]. On this basis, planning studies may provide theoretical RISM risk estimates for modern RT until there is sufficient clinical evidence for the risks of RISM from these new treatment techniques [17-20]. Radiation to normal tissues consists of primary radiation from the treatment beam and secondary radiations from patient scatter, collimator scatter and machine leakage to the out-of-field tissues [15, 17]. A linear dose-response relationship is assumed for risks of RISM in the low dose out-of–field regions [17]. In higher dose, the dose-response relationships are nonlinear [17] and may related to

underlying biological processes including cell transformation, cell killing and cell repopulation [21, 22]. The linear-exponential model (LE) is formulated for the bell-shaped response curve and the linear-plateau model (LP) for curve with high-dose plateau response [17]. Schneider et al [23-25] proposed a concept of organ equivalent dose (OED), a dosimetric index of RISM, which includes dose volume histogram data from the primary beam component and scatter/leakage data for out-of-field component. The concept employs the LE [23] or LP model [24] to define the OED for a specified treatment plan.

Recently, there has been an interest in the use of highly conformal stereotactic body radiotherapy (SBRT) in the treatment of prostate cancer [26]. CyberKnife SBRT (CK-SBRT) in particular offers the physical advantage in precise dose-targeting (highly conformal tumor dose) and accurate dose delivery (with system for tracking organ motion) and the radiobiological advantage of large dose fraction in effective killing of late responding PCa (α/β = 2.7 Gy) [27]. Regarding to the impact of CK-SBRT on RISM risk, CK-SBRT in relative to 3D-CRT generates a larger volume of normal tissues exposed to low doses usually defined at 10% isodose [17] and may contribute to increased RISM risk. In addition, the increased monitor units required for treatment delivery will induce more scatter/leakage doses to out-of-field tissues. Tissues at the immediate vicinity of the irradiated volume may receive doses at intermediate (50% isodose) to high dose levels ($\geq$ 95% isodose) [17]. Pattern of dose distribution to these nearby normal tissues is dependent of the treatment technique. Reduced patient scatter to nearby tissue was estimated for IMRT compared to 3D-CRT [28]. In terms of high doses within the planning target volume (PTV), the risk of in-field sarcoma for CK-SBRT might be lower than 3D-CRT for the difference in size of dose per fraction.

In this study, overall risks of RISM to PTV, organs immediate to the treatment volume, i.e. bladder and rectum in patients with PCa treated by CK-SBRT were compared to risks from 3D-CRT. The OED concept was employed to assess RISM risk from treatment and concomitant imaging doses from tumor tracking in CK-SBRT and from field and setup verifications in 3D-CRT.

CHAPTER II
OBJECTIVES

The main objectives:

1. To determine the total organ equivalent dose (OEDs) including OED_{PTV}, $OED_{bladder}$ and OED_{rectum} of prostate cancer treatment plans for CK-SBRT and 3D-CRT.

2. To evaluate the differences between OEDs (including OED_{PTV}, $OED_{bladder}$ and OED_{rectum}) obtained from CK-SBRT plan and 3D-CRT plan.

The sub-objectives:

1. To determine the differential dose volume histograms (dDVHs) for CK-SBRT and 3D-CRT treatment plans.

2. To determine OEDs (including OED_{PTV}, $OED_{bladder}$ and OED_{rectum}) for the primary beam component of CK-SBRT and 3D-CRT treatment plans.

3. To determine OEDs (including OED_{PTV}, $OED_{bladder}$ and OED_{rectum}) of the scatter/leakage component generated by CK-SBRT and 3D-CRT plans.

4. To determine OEDs (including OED_{PTV}, $OED_{bladder}$ and OED_{rectum}) of the imaging doses for CK-SBRT and 3D-CRT treatments.

5. To determine the total OEDs (including OED_{PTV}, $OED_{bladder}$ and OED_{rectum}) for CK-SBRT and 3D-CRT plans.

CHAPTER III
LITERATURE REVIEWS

3.1 Second cancer risks after radiotherapy

The study of Pickles et al [11] involved 39,261 men with prostate cancer from the British Columbia Tumor Registry. In the cohort, 9,890 of whom received high-dose radiation therapy to the prostate gland (≥ 45 Gy) and 29,371 men who not treated with radiation. Their result showed an increase of 121% for sarcomas and 22% for colo-rectal cancers among patients with prostate cancer who received radiation therapy compared to those without. In addition, the reduce risk of second cancer was observed for bladder cancer among patients who received radiation therapy.

Brenner et al [12] used the data from the Surveillance, Epidemiology, and End Results Programs (SEER) to compare the risk of second cancers in 51,584 men with prostate cancer who received radiotherapy (3,549 of whom developed second cancers) with 70,539 men who received surgery without radiation therapy (5,055 of whom developed second cancers). Their result showed the risk of second cancers was significantly higher after radiotherapy compared to surgery. Particularly for long term survivors, the increase risk with radiotherapy was 15% for patients surviving ≥ 5 years and was 34% for patients surviving ≥ 10 years. The most significant contributors to increase risk in the irradiate group were cancer in organs closed to heavily irradiation sites such as bladder, rectum and in-field sarcomas. In addition, radiotherapy was also an increased risk of lung cancer at distant site. No significant difference between two treatment groups for the risk of out-of-field sarcomas.

In the study of Moon et al [13] involving 140,767 men with prostate cancer who survived ≥5 years after the date of their diagnosis to observe the incidence of second cancers after localized therapy for prostate cancer. Compared with men who were not treated by radiation therapy, men who received external beam radiation therapy (EBRT) as only form of radiation treatment had significantly increased risk of second cancers in several organs which were located within or close to treatment field

like bladder and rectum, as well as organs at sites in the upper body and other areas not potentially related to radiation therapy such as transverse colon, stomach, brain, and lung and bronchus. While men who received radiation therapy in the form of radioactive implants or isotopes either in isolation or in combination with EBRT did not have significantly different for second cancers occurring at these sites.

Diallo et al [16] reported the distribution of second cancer sites in relation to the irradiated volume among 115 patients from a cohort of 4,581 patients who developed a second cancer after childhood cancer radiotherapy. The location of second cancers were classified into three categories of regions, as follows: a. clearly-in-beam region, included second cancers located at more than 2.5 cm inward from the edge of irradiated volume, b. beam-bordering region, included second cancers located in the volume from 2.5 cm inside to 5 cm outside the irradiated volume, c. distant region, included second cancers outward at more than 5 cm from the irradiated volume. According to this classification, 12% of second cancers mostly sarcomas were observed in clearly-in-beam region with median doses 37.1 Gy (7.2 - 63.6), 66% consisted of sarcomas and carcinomas were observed in beam-bordering region with median doses 20.1 Gy (0 - 73.1), while 22% of second cancers mostly carcinomas were observed in distant region with median doses 0.3 Gy (0 – 3). In overall, the most second cancers was 78% observed in clearly-in-beam region and beam-bordering region. Only 22% of these patients were observed in distant region.

3.2 Dose-response relationship for second cancer incidence

A dose-response relationship for radiation-induced cancer is demonstrated as a graph called a dose-response curve. There are two possibilities for the shape of the dose-response curves such as linear-exponential curve and plateau curve. The linear-exponential curve or bell-shaped curve was described by an initiation/inactivation model [21, 22], at low dose the incidence of cancer was a linear function of dose, and then begins to fall at higher dose due to cell killing effect [22] such as bone sarcoma [29] and thyroid cancer [30] as shown in Figure 3.1. While plateau curve, it has not decreased at the higher dose due to cell repopulation during and after radiation therapy which tend to counteract the effect of cell killing [22]. This can be described by

initiation/inactivation/proliferation model [21] such as cancer of breast, bladder and stomach [31] as shown in Figure 3.2.

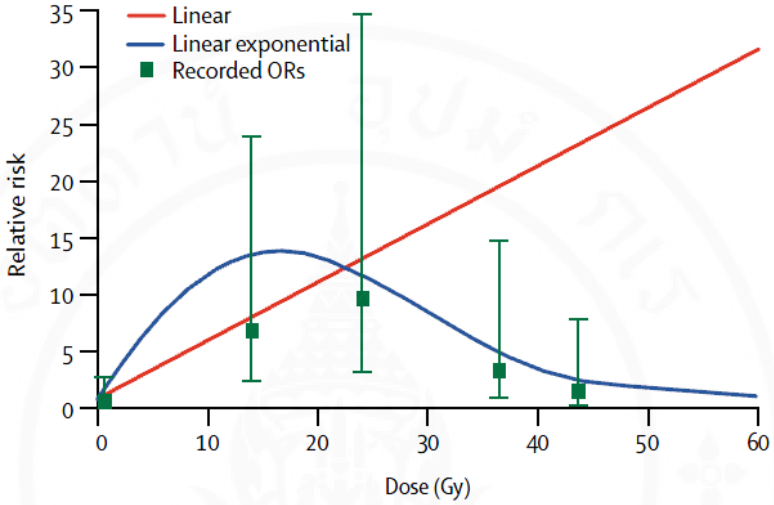

Figure 3.1 The dose-response curve for radiation induced thyroid cancer [30].

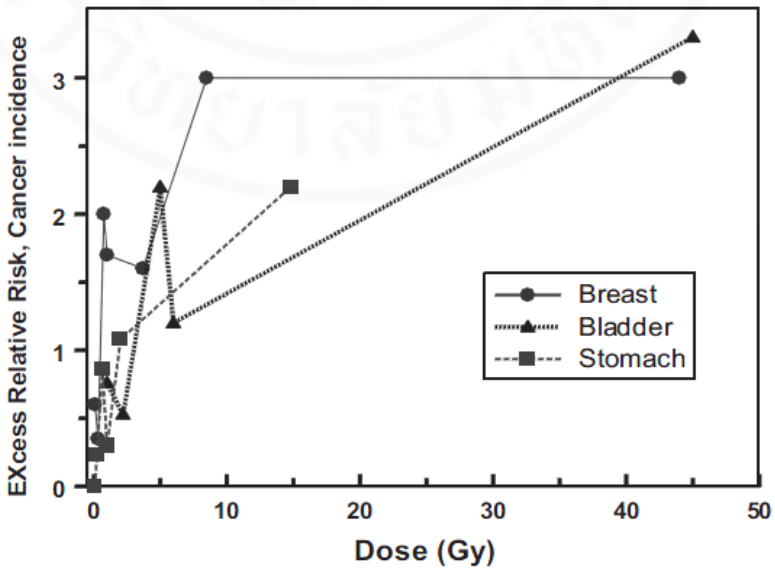

Figure 3.2 The dose-response curve for radiation induced cancer of breast, bladder and stomach after radiotherapy [31].

3.3 Risk estimation of second cancer after radiotherapy

Schneider et al [23-25] proposed a concept of organ equivalent dose (OED) in the estimation of second cancer risk. The basis for the OED model is the dose-response relationship for radiation-induced cancer. In low doses, the OED is simply the average organ dose, since for these doses the dose-response function behaves linearly with dose. However, at high doses is different due to cell killing or cell repopulation. Therefore, the two simulation models to determine the OED at high dose included linear-exponential model (equation 1), and plateau model (equation 2).

Linear-exponential model

$$\mathrm{OED} = \frac{1}{\mathrm{V}} \sum_{\mathrm{i}} \mathrm{V_i}\, \mathrm{D_i}\, \exp(-\alpha \mathrm{D_i}) \qquad (1)$$

Plateau model

$$\mathrm{OED} = \frac{1}{\mathrm{V}} \sum_{\mathrm{i}} \mathrm{V_i} \frac{(1-\exp(-\delta \mathrm{D_i}))}{\delta} \qquad (2)$$

Where α is a linear-exponential model parameter (0.044 Gy^{-1}) [25] and δ is a plateau model parameter (0.139 Gy^{-1}) [25], which were obtained from a combined fit the Japanese atomic bomb survivors and Hodgkin's patients cured by radiotherapy.

Schneider et al [32] used OED in the calculation of radiation-induced second cancers in patients with prostate cancer treated by IMRT and 3D-CRT with 15 MV and 18 MV photon beams. The impacts of primary dose distribution as well as scatter/leakage radiation were analyzed. The differential dose volume histograms (dDVHs) data of the calculated treatment plan were used to determine the OED for primary doses. For the OED of scatter/leakage radiation was obtained from measured data for a point located 50 cm away from the center of treatment field. When compared to the 3D-CRT using the linear-exponential model, an increased risk of second cancer among prostate cancer patients who treated by IMRT was 18.2% for 15 MV and 21.2% for 18 MV observed in OED for primary doses, while 50% for 15 MV

and 43.8% for 18 MV observed in the OED for scatter/leakage radiation. In overall, the total OEDs from IMRT was 1.2 times for 15 MV and 1.3 times for 18 MV higher than from 3D-CRT.

CHAPTER IV
MATERIALS AND METHODS

4.1 Patients

This study included six patients with prostate cancer who were treated at the Radiosurgery Center, Ramathibodi Hospital. Two treatments by CK-SBRT and 3D-CRT were planned for each of six patients. The CK-SBRT treatment was delivered by Accuray CyberKnife G4 System (Accuray Incorporated, Sunnyvale, CA) with a 6 MV linear accelerator (linac) mounted on a computer-controlled robotic arm. The 3D-CRT treatment was delivered by Varian Clinac iX (Varian Medical Systems, Palo Alto, CA) with seven irradiation fields using 10 MV photons. Details for treatment plans are presented in Tables 4.1 and 4.2. This study was approved by the ethic committee of the Faculty of Medicine Ramathibodi Hospital.

4.2 Computerized treatment planning system

The computerized treatment planning system used in CK-SBRT is the MultiPlan® Treatment Planning System (Accuray Incorporated, Sunnyvale, CA). The MultiPlan® system can create the treatment plan which has excellent conformality and coverage made possible by steep dose gradients. The system provides tools necessary to performing a complete range of treatment planning tasks, i.e. from image registration, target and critical structure delineation, through dose optimization, calculation and plan review. The system calculates dose on the basis of the ray tracing algorithm.

The 3D-CRT treatment planning system is the Eclipse version 8.9.15 (Varian Medical Systems, Palo Alto, CA). The Eclipse system uses the Analytical Anisotropic Algorithm (AAA) for dose calculation and also equipped with effective tools to reduce the complexity of contouring tasks, simplify field set up and facilitate a fast calculation which reduces treatment planning time.

4.3 Accuray CyberKnife G4 Systems

Accuray CyberKnife G4 System (Figure 4.1) is used for CK-SBRT treatment. This system uses a 6 MV linear accelerator mounted on a six-axis robotic manipulator and is integrated with an imaging system to localize the target during treatment. The imaging system consists of two ceiling-mounted kilovoltage (kV) X-ray sources and two image detectors mounted on the floor. The field size of radiation beam is determined by a circular collimator with diameters ranging from 5 mm to 60 mm in 12 steps.

Figure 4.1 Accuray CyberKnife G4 system.

4.4 Linear accelerator

The Varian Clinac iX linear accelerator (Figure 4.2) used for 3D-CRT treatment, generates dual photon beam energies of 6 and 10 MV and six electron beam energies of 4, 6, 9, 12, 16, 20 MeV. Field sizes of photon beam range from 0.5x0.5 cm^2 to 40x40 cm^2 at the isocenter and electron beam from 6x6 cm^2 to 25x25 cm^2. The distance from the source of the treatment machine to the isocenter is 100 cm. There are six stationary therapy dose rates ranging from 100 to 600 monitor units per minute.

The imaging system uses the megavoltage treatment beam as imaging source and the electronic portal imaging device (EPID) mounted on the linear accelerator for image capture. This imaging system is capable of creating two-dimensional electronic images used for the patient setup verification and individual field placement verification.

Figure 4.2 Varian Clinac iX linear accelerator.

4.5 The Alderson Rando Phantom

The Alderson Rando phantom (Figure 4.3) was used to measure the scatter/leakage doses and imaging doses. The size of phantom is a 155 cm tall and weighed 50 kg. The phantom consists of tissue-equivalent materials which are transected horizontally into slabs of 2.5 cm thickness. Each slice contains a matrix of holes with 5 mm in diameter spacing 1 cm apart. These holes are filled with bone-equivalent, soft tissue-equivalent or lung tissue-equivalent pins in relevant locations and the pins can be replaced by TLD.

Figure 4.3 The Alderson Rando phantom.

4.6 Thermoluminescence dosimeter (TLD) system

4.6.1 Thermoluminescence dosimeter (TLD-700)

The TLD-700 (Harshaw Chemical Company) in the form of rod, with 1 mm diameter and 5 mm long (Figure 4.4), was used to measure the scatter/leakage radiations from CK-SBRT and 3D-CRT technique and the imaging doses from 3D-CRT technique. The dosimeter is lithium fluoride (LiF) crystals doped with magnesium and titanium (LiF:Mg,Ti). The TLD-700 consists of ^{6}Li (0.01%) and ^{7}Li (99.99%). The useful dose range of the TLD-700 is 10μGy-10Gy [33].

Figure 4.4 Array of thermoluminescence dosimeter (TLD-700) in the TLD planchet.

4.6.2 Thermoluminescence dosimeter (TLD-100H)

The TLD-100H (Harshaw Chemical Company) in the form of a square chip with a size of 3.2 mm x 3.2 mm x 0.38 mm and a density of 2.48 g/cm^3 (Figure 4.5), was used to measure the imaging doses from CK-SBRT technique. The dosimeter is lithium fluoride (LiF) crystals doped with magnesium, copper and phosphorus (LiF:Mg,Cu,P). The TLD-100H consists of ^{6}Li (7.36%) and ^{7}Li (92.14%). The useful dose range of the TLD-100H is 1 µGy-20 Gy [34].

Figure 4.5 Array of thermoluminescence dosimeter (TLD-100H) in the TLD planchet.

4.6.3 Thermoluminescence reader

The automatic TLD reader is Harshaw model 5500 with TLD Shell software (Figure 4.6). The reader uses a hot nitrogen gas heating system and the heating temperature is controlled by the WinREMS software. The temperature controlled software run by a Window operating system is a closed loop feedback capable of producing linearity ramped temperature up to 400 ^{o}C with the accuracy of ± 1 ^{o}C. The TLD reader can be calibrated in gray or sieverts with different scales. It can be used for various types of TLD.

Figure 4.6 The automatic TLD reading system.

4.6.4 TLD annealing oven

The TLD annealing oven (Figure 4.7) is equipped with two standard programs for annealing and preheating. Annealing program is used for annealing TLD before irradiation, while preheating program is used for preheating TLD before reading. The oven temperature is adjusted by the TLDO software.

Figure 4.7 The TLD annealing oven.

4.7 Treatment planning

CT scan or MRI from each patient were recorded in DICOM standard format and imported to MultiPlan® treatment planning system of CK-SBRT and to Eclipse treatment planning system (version 8.9.15) of 3D-CRT. Dose distributions between PTV, bladder and rectum were calculated based on contours drawn by the oncologist. The PTV for CK-SBRT was defined as the GTV plus 5 mm in all directions except for the posterior margin which was set at 3 mm. For 3D-CRT, the margin of PTV was assigned at 7 mm from GTV in all directions except for posterior which was set at 5 mm. The optimized CK-SBRT plan was the plan capable of delivery a prescribed dose of 36.25 Gy to the PTV in 5 fractions of 7.25 Gy without violating the dose constraints of bladder (<15 ml and maximum point dose 38 Gy) and rectum (<20 ml and maximum point dose 38 Gy) as suggested by Timmerman [35]. For 3D-CRT, the plan with seven irradiation fields using 10 MV photons was optimized to deliver the prescribed dose of 76 Gy to the PTV in 38 fractions of 2 Gy without violating the dose constraints to bladder and rectum as suggested by Ramathibodi protocol. Parameters involving treatment delivery such as energy, beam

orientation, collimator size, treatment MUs, etc. were described in Tables 4.1 and 4.2.

Table 4.1 The CK-SBRT treatment plans for six patients with prostate cancer.

	Case					
Variable	**Pt 1**	**Pt 2**	**Pt 3**	**Pt 4**	**Pt 5**	**Pt 6**
GTV (cm^3)	62.01	44.42	44.88	43.71	55.11	36.64
PTV (cm^3)	95.84	84.25	84.81	78.61	97.96	69.23
Beam energy (MV)	6	6	6	6	6	6
Prescribe dose (Gy)	36.25	36.25	36.25	36.25	36.25	36.25
Dose/fraction (Gy)	7.25	7.25	7.25	7.25	7.25	7.25
Number of fraction	5	5	5	5	5	5
Collimator size(mm)	15, 35	15, 30	20, 30	20, 35	15, 30	12.5, 35
No.beam orientation	289	285	184	252	245	246
Max dose (Gy)	45.31	45.31	45.89	44.75	44.75	45.31
Total treatment MU	40175	50488.4	40615.92	35294.95	50420.47	48574.63
No. imaging beams	1275	1220	1015	1195	1145	880

Table 4.2 The 3D-CRT treatment plans for six patients with prostate cancer.

Variable	Case					
	Pt 1	**Pt 2**	**Pt 3**	**Pt 4**	**Pt 5**	**Pt 6**
GTV (cm^3)	62.01	44.42	44.88	43.71	55.11	36.64
PTV (cm^3)	133.16	107.66	108.08	109.19	120.93	92.89
Beam energy (MV)	10	10	10	10	10	10
Prescribe dose (Gy)	76	76	76	76	76	76
Dose/fraction (Gy)	2	2	2	2	2	2
Number of fraction	38	38	38	38	38	38
Max field size (cm)	8.3 X 7.6	7.8 X 8.0	8.4 X 7.1	8.5 X 6.9	8.4 X 7.2	8.1 X 5.8
No. beam orientation	7	7	7	7	7	7
Max dose (Gy)	78.38	79.1	79.95	79.71	79.07	79.34
Total treatment MU	10868	11438	10868	11020	11628	12350
No. imaging beams	21	21	21	21	21	21

4.8 Determination of the total organ equivalent dose (OED_T)

The total organ equivalent dose (OED_T) for PTV, bladder and rectum from CK-SBRT and 3D-CRT treatment plans were described by equation 3.

$$OED_T = OED_{prim} + OED_{scatter/leakage} + OED_{image} \quad (3)$$

Where OED_{prim} = organ equivalent dose for primary beam.

$OED_{scatter/leakage}$ = organ equivalent dose for scatter/leakage radiation.

OED_{image} = organ equivalent dose for imaging doses.

4.8.1 Determination of the OED primary for primary beam component

OED of the primary beam component is the equivalent dose defined for organs in volume of CT scan [32].

a. OED primary for PTV ($OED_{prim,\ PTV}$)

$$OED_{prim,\ PTV} = \frac{1}{V_{PTV}} \sum_i dDVH\ D_i e^{-\alpha D_i} \quad (4)$$

Where V_{PTV} = total organ volume in cm^3 for PTV.

dDVH = differential dose volume histogram in corresponding to D_i, dDVH was calculated at 1% dose gradient for CK-SBRT and 0.2 Gy dose gradient for 3D-CRT.

α = 0.044 Gy^{-1} a model parameter describing cell killing [25].

b. OED primary for bladder ($OED_{prim,\ blad}$)

$$OED_{prim,\ blad} = OED_{in\ PTV} + OED_{out\ PTV}$$

$$= \left[\frac{1}{V_{blad}} \sum_i dDVH\ D_i e^{-\alpha D_i}\right]_{in\ PTV} + \left[\frac{1}{V_{blad}} \sum_i dDVH\ \frac{(1-e^{-\delta D_i})}{\delta}\right]_{out\ PTV} \quad (5)$$

Where V_{blad} = total organ volume in cm^3 for bladder.

dDVH = differential dose volume histogram in corresponding to D_i, dDVH was calculated at 1% dose gradient for CK-SBRT and 0.2 Gy dose gradient for 3D-CRT.

α = 0.044 Gy^{-1} a model parameter describing cell killing [25].

δ = 0.139 Gy^{-1} a model parameter describing cell repopulation [25].

c. OED primary for rectum ($OED_{prim,\ rec}$)

$$OED_{prim,\ rec} = OED_{in\ PTV} + OED_{out\ PTV}$$

$$= \left[\frac{1}{V_{rec}}\sum_i dDVH\ D_i e^{-\alpha D_i}\right]_{\text{in PTV}} + \left[\frac{1}{V_{rec}}\sum_i dDVH\ \frac{(1-e^{-\delta D_i})}{\delta}\right]_{\text{out PTV}} \quad (6)$$

Where V_{rec} = total organ volume in cm^3 for rectum.

dDVH = differential dose volume histogram in corresponding to D_i, dDVH was calculated at 1% dose gradient for CK-SBRT and 0.2 Gy dose gradient for 3D-CRT.

α = 0.044 Gy^{-1} a model parameter describing cell killing [25].

δ = 0.139 Gy^{-1} a model parameter describing cell repopulation [25].

To account for the biological difference in different dose per fraction used for CK-SBRT and 3D-CRT treatment, all D_i's from DVH data were normalized to an equivalent dose in 2 Gy per fractions (EQD_2) which described by equation 7.

$$EQD_2 = D_i\left[\frac{d_i + \alpha/\beta}{2 + \alpha/\beta}\right] \quad (7)$$

Where D_i = dose associated with the $dDVH_i$.

d_i = D_i/fraction number, the fraction number was 5 and 38 for CK-SBRT and 3D-CRT, respectively.

α/β = 2.7 Gy for prostate [27], 10 Gy for bladder and rectal complication [36, 37].

4.8.2 Determination of the $OED_{scatter/leakage}$

a. The $OED_{scatter/leakage}$ for CK-SBRT and 3D-CRT treatment plans was calculated by plateau model which described by equation 8.

$$OED_{scatter/leakage} = \frac{V_T}{V_{WB}}\frac{(1-e^{-\delta \bar{D}_{WB}})}{\delta} \quad (8)$$

Where V_T was whole volume of PTV, bladder and rectum, and V_{WB} was the whole body volume receiving scatter/leakage dose (D_{SL}) of D Gy which calculated

from the patient whole body weight (WB) in g , with a body density (G) of 1.07 g/cm^3 for male [38] which defined by equation 9.

$$V_{WB} = \frac{WB}{G} \ (cm^3) \quad (9)$$

b. Scatter/leakage dose from treatment (D_{SL}) was measured for each treatment plan. Firstly, TLD-700 rods were placed in ten positions within the Rando phantom. The ten measured positions were outside the treatment field (Figure 4.8). Points of measurement in the Rando phantom are shown in Table 4.3. The phantom was setup exactly the same position as the patient was treated. Scatter/leakage doses from CK-SBRT plans were measured by irradiating the phantom with a dose of 5 Gy from 6 MV photons and for 3D-CRT plans with a dose of 10 Gy from 10 MV photons. The measurements were repeated 3 times. The scatter/leakage dose was calculated by dividing individual TLD dose with the total MU used in phantom irradiation. The Gy/MU was a unit of the scatter/leakage dose which measured by TLD divided by the total MU which used for the calculation of whole body dose from scatter/leakage radiation. The scatter/leakage dose from the treatment (D_{SL}) was Gy/MU for total body multiplied by the total MU used for treatment.

Table 4.3 Points of measurement for scatter/leakage dose in Rando phantom.

Organ	Slab number	Distance from tumor center (cm.)
Brain	2	70
Right and left thyroid	8	54
Right and left lung	14	38.8
Sternum	14	39.4
Liver	18	28.5
Stomach	18	25.5
Right and left kidney	21	20.7

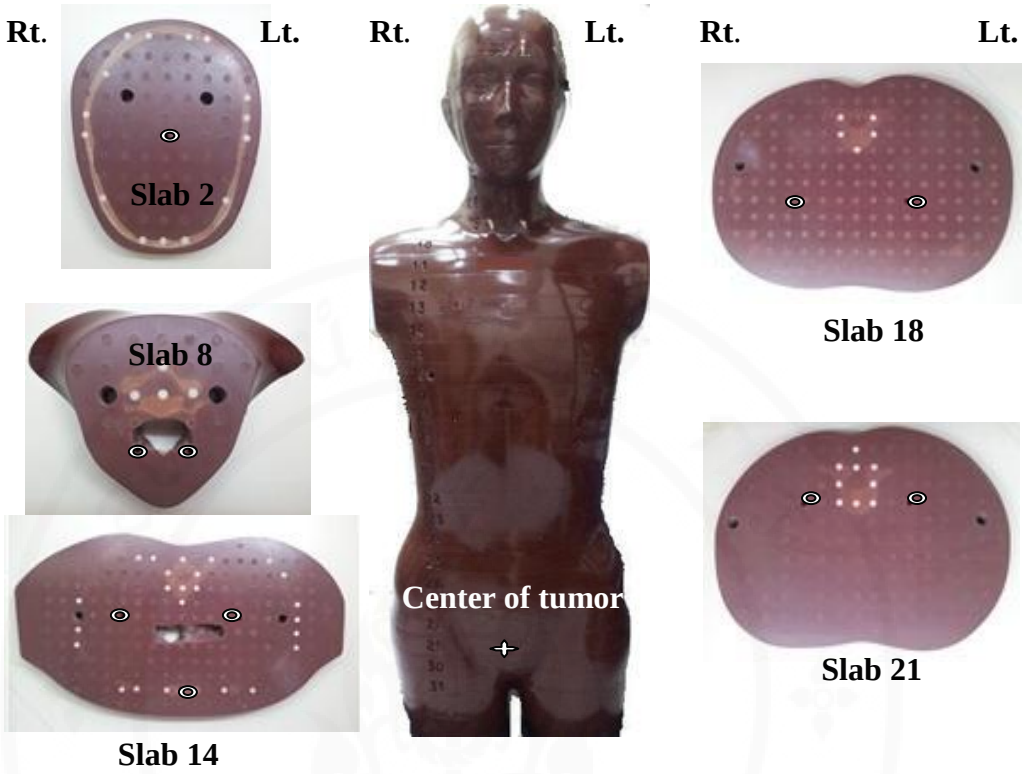

Figure 4.8 Positions of TLD in Rando phantom for the scatter/leakage dose measurement.

4.8.3 Determination of the OED_{image}

a. The OED_{image} for CK-SBRT and 3D-CRT treatment plans were calculated by plateau model which described by equation 10.

$$OED_{image} = \frac{(1-e^{-\delta \bar{D}_{image}})}{\delta} \quad (10)$$

b. Using the Rando phantom, the imaging doses were measured with TLD-100H chips for CK-SBRT treatment plans and TLD-700 rods for 3D-CRT treatment plans. TLDs were placed at 15 positions in the Rando phantom (Figure 4.9). Points of measurement in the Rando phantom are shown in Table 4.4. The phantom was setup the same position as patients were treated. For CK-SBRT, the exposure technique for imaging the target location was 120 kV, 100 mA and 100 ms (10 mAs) for each image. A total of 150 exposures were given per each imaging dose measurement.

In 3D-CRT, each patient received doses from image verification protocol, for seven treatment fields and anterior-posterior plus lateral setup. Imaging for treatment field and setup verification was performed by the EPID system used a double exposure technique (MLC versus open field) with a low dose mode (1MU/image). Imaging doses were measured from cumulative doses of five repeated image verification protocols. The measurement was repeated 3 times.

Table 4.4 Points of measurement for image dose in the Rando phantom.

Organ/location	Points of measurement
Brain	1
Right and left thyroid	2, 3
Right and left lung	4, 5
Sternum	6
Liver	7
Stomach	8
Right and left kidney	9, 10
Bladder	11
Rectum	12
Tumor center	13
Skin dose	14, 15

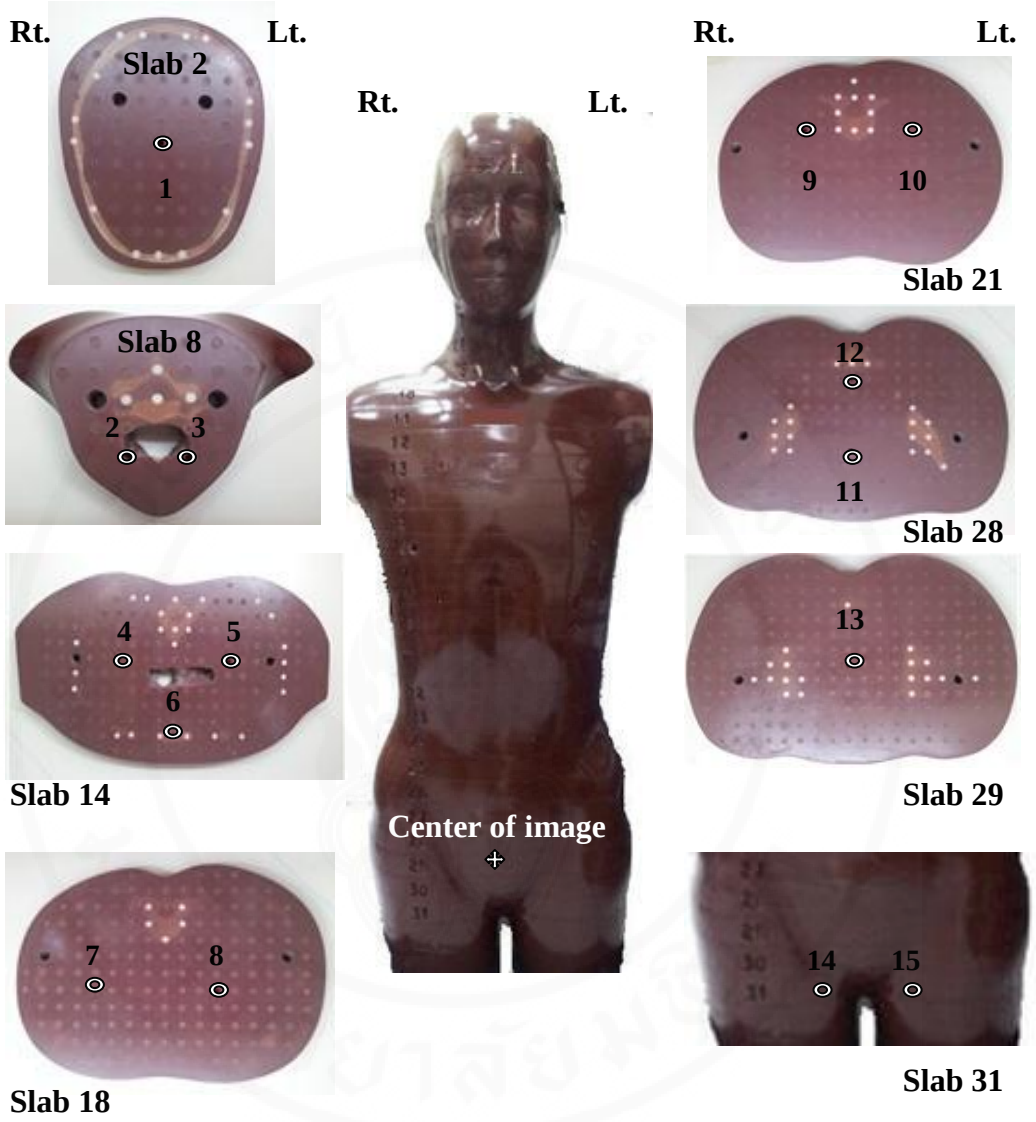

Figure 4.9 Positions of TLD in Rando phantom for the image dose measurement.

4.9 Statistical analysis

Student t-test [39] was used to analyze the difference in OED from CK-SBRT and 3D-CRT treatment plans. All of the statistical tests were two-tailed, and $p \leq 0.05$ was considered statistically significant.

CHAPTER V
RESULTS

5.1 OED determination for primary beam component

5.1.1 EQD_2 calculation

Physical doses from the differential dose volume histograms (dDVHs) of CK-SBRT and 3D-CRT treatment plans were converted to EQD_2 using equation 7. Organs at risks were PTV, bladder and rectum. EQD_2 for PTV treated by CK-SBRT and 3D-CRT are presented in Table 5.1. Parts of bladder and rectum included in PTV and outside PTV, EQD_2's were calculated using α/β of 10 Gy [36, 37] (Tables 5.2 and 5.3).

Table 5.1 EQD_2 for PTV treated by CK-SBRT and 3D-CRT.

Patient code	CK-SBRT		3D-CRT	
	Volume, cm^3	Dose weighted by volume*, Gy	Volume, cm^3	Dose weighted by volume*, Gy
1	95.84	90.8664	133.16	77.5489
2	84.25	90.0045	107.66	77.7959
3	84.80	91.9163	108.08	79.2906
4	78.61	88.3306	109.19	78.6738
5	97.96	89.9595	120.93	78.1262
6	69.23	91.3027	92.89	78.3888
Average (SD)	85.12 (10.73)	90.3967 (1.2621)	111.99 (13.67)	78.3040 (0.6289)

*Dose weighted by volume $= \frac{\sum \mathrm{dDVHi} \times \mathrm{EQD}_2^{\mathrm{i}}}{\mathrm{V_{PTV}}}$

Table 5.2 EQD_2 for bladder treated by CK-SBRT and 3D-CRT.

Patient code	Volume, cm^3	Dose weighted by volume*, Gy			
		CK-SBRT		3D-CRT	
		$Bladder_{inPTV}$	$Bladder_{outPTV}$	$Bladder_{inPTV}$	$Bladder_{outPTV}$
1	162.82	1.4431	23.7633	5.8151	31.8054
2	124.05	0.2316	18.2335	3.3125	25.7936
3	165.19	0.2724	17.2824	3.5058	26.4440
4	149.89	0.3644	19.4068	3.2306	25.2666
5	164.61	0.7786	19.4745	3.5385	21.7669
6	164.04	0.5399	10.3973	2.7977	12.8322
Average	155.1	0.6050	18.0930	3.7000	23.9848
(SD)	(16.27)	(0.4571)	(4.3746)	(1.0698)	(6.3470)

*Dose weighted by volume $= \frac{\sum \mathrm{dDVHi} \times \mathrm{EQD}_2^{\mathrm{i}}}{\mathrm{V}_{\mathrm{total\ bladder}}}$

Table 5.3 EQD_2 for rectum treated by CK-SBRT and 3D-CRT.

Patient code	Volume, cm^3	Dose weighted by volume*, Gy			
		CK-SBRT		3D-CRT	
		$Rectum_{inPTV}$	$Rectum_{outPTV}$	$Rectum_{inPTV}$	$Rectum_{outPTV}$
1	70.64	0.2916	17.9417	2.6355	32.2453
2	273.95	0.5283	14.0013	1.6744	25.4665
3	69.60	0.6607	18.7690	3.3591	34.6332
4	90.55	0.1816	17.7446	2.3670	26.3779
5	100.61	0.5688	21.7811	1.3666	33.0382
6	44.45	0.1105	14.5660	1.4420	28.0228
Average	108.3	0.3903	17.4673	2.1408	29.9640
(SD)	(83.43)	(0.2261)	(2.8648)	(0.7855)	(3.8292)

*Dose weighted by volume $= \frac{\sum \mathrm{dDVHi} \times \mathrm{EQD}_2^{\mathrm{i}}}{\mathrm{V}_{\mathrm{total\ rectum}}}$

5.1.2 Calculation of OED primary (OED_{prim})

OED_{prim} in PTV was calculated using linear-exponential model and outside PTV using plateau model. OED_{prim}'s for PTV, bladder and rectum were calculated using equations 4, 5, 6, respectively and are presented in Tables 5.4-5.6.

Table 5.4 OED_{prim} for PTV treated by CK-SBRT and 3D-CRT.

Patients code	CK-SBRT (LE model), Gy	3D-CRT (LE model), Gy
1	1.746	2.5582
2	1.7581	2.5397
3	1.6671	2.4239
4	1.8586	2.4712
5	1.7627	2.5132
6	1.7126	2.4933
Average	1.7509	2.4999
(SD)	(0.0637)	(0.0486)

Table 5.5 OED_{prim} for bladder treated by CK-SBRT and 3D-CRT.

Patient code	CK-SBRT			3D-CRT		
	$Bladder_{inPTV}$ (LE model), Gy	$Bladder_{outPTV}$ (LP model), Gy	Total, Gy	$Bladder_{inPTV}$ (LE model), Gy	$Bladder_{outPTV}$ (LP model), Gy	Total, Gy
1	0.1353	6.4921	6.6274	0.1978	5.6291	5.8269
2	0.021	6.1246	6.1456	0.1118	5.6577	5.7695
3	0.0265	5.8378	5.8643	0.1136	5.3264	5.44
4	0.0358	6.105	6.1408	0.1027	5.1295	5.2322
5	0.0691	5.8656	5.9347	0.1214	4.8389	4.9603
6	0.0488	4.43	4.4788	0.0975	3.416	3.5135
Average	0.0561	5.8092	5.8653	0.1241	4.9996	5.1237
(SD)	(0.0425)	(0.7155)	(0.7297)	(0.0371)	(0.8351)	(0.8536)

Table 5.6 OED_{prim} for rectum treated by CK-SBRT and 3D-CRT.

Patient code	CK-SBRT			3D-CRT		
	$Rectum_{inPTV}$ (LE model), Gy	$Rectum_{outPTV}$ (LP model), Gy	Total, Gy	$Rectum_{inPTV}$ (LE model), Gy	$Rectum_{outPTV}$ (LP model), Gy	Total, Gy
1	0.0348	6.0791	6.1139	0.0885	5.8467	5.9352
2	0.046	5.0192	5.0652	0.0575	5.5132	5.5707
3	0.0644	5.8491	5.9135	0.1049	5.7321	5.837
4	0.0184	5.0653	5.0837	0.0777	4.5485	4.6262
5	0.0591	6.1823	6.2414	0.046	5.5955	5.6415
6	0.0123	4.8506	4.8629	0.0478	4.4797	4.5275
Average	0.0392	5.5076	5.5468	0.0704	5.286	5.3564
(SD)	(0.0212)	(0.594)	(0.6087)	(0.0238)	(0.6091)	(0.6186)

Table 5.7 shows the OED_{prim} for PTV, bladder and rectum from CK-SBRT compared with 3D-CRT. The paired t-test was used to test for the difference between the two treatment plans. $OED_{prim,\ PTV}$ from 3D-CRT was significantly higher than that from CK-SBRT whereas $OED_{prim,\ blad}$ was lower. No significant difference between two treatment plans could be observed for $OED_{prim,\ rec.}$

Table 5.7 Comparison between OED_{prim}'s from CK-SBRT and 3D-CRT.

Organ	CK-SBRT $\bar{X}$(SD), Gy	3D-CRT $\bar{X}$(SD), Gy	$\frac{CK-SBRT}{3D-CRT}$	P-value
PTV	1.7509 (0.0637)	2.4999 (0.0486)	0.7004 (0.0289)	<< 0.0001
Bladder	5.8653 (0.7297)	5.1237 (0.8536)	1.1447 (0.2380)	0.001
Rectum	5.5468 (0.6087)	5.3564 (0.6186)	1.0355 (0.1650)	0.284

5.2 Scatter and leakage dose component

5.2.1 Scatter/leakage dose (D_{SL})

Scatter/leakage dose (D_{SL}) to total body was estimated from measured data in ten positions outside the treatment field (Table 5.8). Firstly, dose in each of the ten positions was divided by total MU used in phantom irradiation to obtain the scatter/leakage dose in Gy/MU. Then doses measured at ten positions in Rando phantom was averaged to obtain the scatter/leakage dose to the whole body [40]. Scatter/leakage doses (D_{SL}) from treatment at ten positions are presented in Table 5.9. For each patient, the scatter/leakage dose from the treatment (D_{SL}) was the whole body dose in Gy/MU multiplied by the total treatment monitor unit (MU) for each patient as shown in Table 5.10.

Table 5.8 Scatter/leakage dose (Gy/MU) from TLD measurement in 10 positions outside the treatment field from CK-SBRT and 3D-CRT.

Organ	Distance from tumor center, cm	Scatter/leakage dose, Gy/MU	
		CK-SBRT $\bar{X}$(SD)	3D-CRT $\bar{X}$(SD)
Brain	70	2.21E-06 (1.00E-08)	2.06E-06 (8.96E-08)
Right thyroid	54	3.06E-06 (1.66E-08)	2.52E-06 (4.77E-08)
Left thyroid	54	2.93E-06 (4.65E-08)	2.29E-06 (3.44E-08)
Right lung	38.8	2.20E-06 (1.45E-08)	2.88E-06 (5.54E-08)
Left lung	38.8	2.07E-06 (2.36E-08)	2.73E-06 (1.30E-07)
Sternum	39.4	2.58E-06 (1.76E-08)	3.30E-06 (4.07E-08)
Liver	28.5	2.30E-06 (1.02E-08)	5.01E-06 (6.13E-08)
Stomach	25.5	2.15E-06 (3.57E-08)	4.65E-06 (1.81E-08)
Right kidney	20.7	2.97E-06 (2.32E-08)	1.34E-05 (5.84E-08)
Left kidney	20.7	2.99E-06 (1.27E-08)	1.53E-05 (8.39E-08)
Whole body		2.48E-06 (4.86E-09)	4.55E-06 (1.28E-08)

Table 5.9 Scatter/leakage dose (D_{SL}) to organ outside the treatment field at 10 positions from CK-SBRT and 3D-CRT.

Organ	Distance from tumor center, cm	Scatter/leakage dose, Gy	
		CK-SBRT $\bar{X}$(SD)	3D-CRT $\bar{X}$(SD)
Brain	70	0.0896 (0.0004)	0.0230 (0.0010)
Right thyroid	54	0.1481 (0.0008)	0.0296 (0.0006)
Left thyroid	54	0.1263 (0.0020)	0.0264 (0.0004)
Right lung	38.8	0.0815 (0.0006)	0.0326 (0.0006)
Left lung	38.8	0.0922 (0.0011)	0.0307 (0.0015)
Sternum	39.4	0.1178 (0.0008)	0.0361 (0.0004)
Liver	28.5	0.1014 (0.0004)	0.0559 (0.0007)
Stomach	25.5	0.1008 (0.0017)	0.0520 (0.0002)
Right kidney	20.7	0.1216 (0.0009)	0.1545 (0.0007)
Left kidney	20.7	0.1485 (0.0007)	0.1740 (0.0009)
Whole body		0.1052 (0.0002)	0.0510 (0.0001)

Scatter/leakage dose from treatment (D_{SL}) at ten positions ranged from 0.0815 to 0.1485 Gy, with an average dose to whole body of 0.1052 Gy (SD = 0.0002) for CK-SBRT plan. For 3D-CRT plan, the scatter/leakage dose ranged from 0.0230 to 0.1740 Gy with an average dose to whole body of 0.0510 Gy (SD = 0.0001). Scatter/leakage dose from CK-SBRT plan was 2.06 times higher than from 3D-CRT plan ($p = 0.0086$, by paired t-test).

Table 5.10 Whole body scatter/leakage doses (D_{SL}) from CK-SBRT and 3D-CRT.

Patient code	Whole body volume, cm^3	CK-SBRT			3D-CRT		
		Gy/MU (SD)	Total MU	D_{SL}(SD), Gy	Gy/MU (SD)	Total MU	D_{SL}(SD), Gy
1	53271.03	2.69E-06 (2.89E-08)	40175	0.1084 (0.0012)	3.85E-06 (4.09E-08)	10868	0.0419 (0.0004)
2	81869.16	2.66E-06 (7.61E-09)	50488.4	0.1336 (0.0004)	3.94E-06 (4.98E-08)	11438	0.0448 (0.0006)
3	54018.69	2.31E-06 (9.01E-09)	40615.92	0.0938 (0.0004)	5.38E-06 (5.04E-08)	10868	0.0582 (0.0005)
4	63831.78	2.30E-06 (1.21E-08)	35294.95	0.0813 (0.0004)	4.47E-06 (1.88E-08)	11020	0.0497 (0.0002)
5	70280.37	2.46E-06 (2.88E-08)	50420.47	0.1243 (0.0014)	5.24E-06 (2.91E-08)	11628	0.0598 (0.0003)
6	67943.93	2.42E-06 (1.71E-08)	48574.63	0.1183 (0.0008)	4.25E-06 (3.65E-08)	12350	0.0528 (0.0005)
Average (SD)	65202.49 (10773.99)	2.48E-06 (4.86E-09)	44261.56 (6414.03)	0.1052 (0.0002)	4.55E-06 (1.28E-08)	11362 (575.8)	0.051 (0.0001)

5.2.2 Calculation of OED scatter/leakage ($OED_{scatter/leakage}$)

$OED_{scatter/leakage}$'s for PTV, bladder and rectum were calculated using the equation 8. The results are shown in Tables 5.11-5.13.

Table 5.11 PTV $OED_{scatter/leakage}$ for CK-SBRT and 3D-CRT plans.

Patient code	Whole body volume, cm^3	CK-SBRT		3D-CRT	
		Volume, cm^3	OED, Gy	Volume, cm^3	OED, Gy
1	53271.03	95.84	2.11E-04 (5.75E-06)	133.16	1.67E-04 (5.61E-06)
2	81869.16	84.25	1.35E-04 (1.81E-06)	107.66	7.62E-05 (7.46E-07)
3	54018.69	84.80	1.55E-04 (3.96E-06)	108.08	1.18E-04 (1.83E-06)
4	63831.78	78.61	1.15E-04 (3.29E-06)	109.19	9.98E-05 (9.22E-07)
5	70280.37	97.96	1.76E-04 (6.74E-06)	120.93	1.06E-04 (4.18E-07)
6	67943.93	69.23	1.23E-04 (5.29E-06)	92.89	8.97E-05 (1.98E-06)
Average (SD)	65202.49 (10773.99)	85.12 (10.73)	1.39E-04 (1.35E-06)	111.99 (13.67)	9.96E-05 (3.28E-07)

Table 5.12 Bladder $OED_{scatter/leakage}$ for CK-SBRT and 3D-CRT plans.

Patient code	Volume, cm^3		CK-SBRT	3D-CRT
	Whole body	Bladder		
1	53271.03	162.82	3.58E-04 (9.77E-06)	2.04E-04 (6.86E-06)
2	81869.16	124.05	1.99E-04 (2.66E-06)	8.79E-05 (8.60E-07)
3	54018.69	165.19	3.01E-04 (7.71E-06)	1.80E-04 (2.79E-06)
4	63831.78	149.89	2.20E-04 (6.28E-06)	1.37E-04 (1.27E-06)
5	70280.37	164.61	2.96E-04 (1.13E-05)	1.44E-04 (5.69E-07)
6	67943.93	164.04	2.92E-04 (1.25E-05)	1.58E-04 (3.49E-06)
Average (SD)	65202.49 (10773.99)	155.1 (16.27)	2.24E-04 (2.19E-06)	1.30E-04 (4.35E-07)

Table 5.13 Rectum $OED_{scatter/leakage}$ for CK-SBRT and 3D-CRT plans.

Patient code	Volume, cm^3		CK-SBRT	3D-CRT
	Whole body	Rectum		
1	53271.03	70.64	1.55E-04	8.85E-05
			(4.24E-06)	(2.98E-06)
2	81869.16	273.95	4.38E-04	1.94E-04
			(5.88E-06)	(1.90E-06)
3	54018.69	69.60	1.27E-04	7.58E-05
			(3.25E-06)	(1.18E-06)
4	63831.78	90.55	1.33E-04	8.28E-05
			(3.79E-06)	(7.65E-07)
5	70280.37	100.61	1.81E-04	8.82E-05
			(6.92E-06)	(3.48E-07)
6	67943.93	44.45	7.92E-05	4.29E-05
			(3.40E-06)	(9.47E-07)
Average	65202.49	108.3	1.49E-04	8.50E-05
(SD)	(10773.99)	(83.43)	(1.68E-06)	(2.86E-07)

Comparison between CK-SBRT and 3D-CRT plans revealed that $OED_{scatter/leakage}$'s for PTV, bladder and rectum. For CK-SBRT plans were greater than these of 3D-CRT plans (Table 5.14).

Table 5.14 Comparison between $OED_{scatter/leakage}$'s from CK-SBRT and 3D-CRT.

Organ	CK-SBRT $\bar{X}$(SD), Gy	3D-CRT $\bar{X}$(SD), Gy	$\frac{CK-SBRT}{3D-CRT}$	P-value
PTV	1.39E-04	9.96E-05	1.3956	0.003
	(1.35E-06)	(3.28E-07)	(0.0143)	
Bladder	2.24E-04	1.30E-04	1.7231	<< 0.0001
	(2.19E-06)	(4.35E-07)	(0.0178)	
Rectum	1.49E-04	8.50E-05	1.7529	0.036
	(1.68E-06)	(2.86E-07)	(0.0206)	

5.3 Imaging dose component

5.3.1 Imaging dose

Imaging dose was estimated from measured data in Rando phantom. For CK-SBRT, the exposure technique was 120 kV, 10 mAs. Image doses from 150 exposures measured at 15 positions are shown in Table 5.15.

Table 5.15 Image doses from 150 exposures in 15 positions for CK-SBRT technique with exposure technique set at 120 kV, 10 mAs. Data are means (SD).

Organ	Image dose (Gy)		
	150 images	1 image	Total treatment
Outside the image field			
Brain	8.75E-05	5.84E-07	0.0006
	(1.04E-05)	(6.91E-08)	(3.09E-05)
Right thyroid	3.14E-04	2.09E-06	0.0023
	(3.38E-05)	(2.25E-07)	(0.0001)
Left thyroid	3.24E-04	2.16E-06	0.0023
	(3.43E-05)	(2.29E-07)	(0.0001)
Right lung	4.62E-04	3.08E-06	0.0033
	(4.78E-05)	(3.19E-07)	(0.0001)
Left lung	4.03E-04	2.69E-06	0.0029
	(3.70E-05)	(2.47E-07)	(0.0001)
Sternum	3.60E-04	2.40E-06	0.0026
	(2.85E-05)	(1.90E-07)	(0.0001)
Inside the image field			
Liver	0.0012	7.94E-06	0.0086
	(0.0002)	(1.31E-06)	(0.0006)
Stomach	0.0015	9.96E-06	0.0108
	(0.0001)	(7.65E-07)	(0.0003)
Right kidney	0.0048	3.23E-05	0.035
	(0.0006)	(4.21E-06)	(0.0019)
Left kidney	0.0062	4.15E-05	0.045
	(0.0011)	(7.55E-06)	(0.0034)
Bladder	0.0369	2.46E-04	0.2666
	(0.0034)	(2.24E-05)	(0.01)
Rectum	0.0091	6.04E-05	0.0655
	(0.0012)	(8.12E-06)	(0.0036)
Tumor center	0.019	1.26E-04	0.1369
	(0.0033)	(2.20E-05)	(0.0098)
*Skin dose	0.097	6.46E-04	0.7013
	(0.0013)	(8.87E-06)	(0.004)

Imaging doses outside the image field for total treatment ranged from 0.0006 to 0.0033 Gy while inside the image field ranged from 0.0086 to 0.1369 Gy. Organ of interest such as PTV, bladder and rectum for each patient was different according to the number of images taken for the whole treatment which were calculated based on a single image dose as shown in Table 5.15. The results of calculate for each patient are shown in Table 5.16.

Table 5.16 Imaging doses estimated for PTV, bladder and rectum in CK-SBRT treatment.

Patient code	Image number	PTV		Bladder		Rectum	
		Dose/image	Total dose	Dose/image	Total dose	Dose/image	Total dose
1	1275	1.26E-04 (2.20E-05)	0.1612 (0.028)	2.46E-04 (2.24E-05)	0.3135 (0.0286)	6.04E-05 (8.12E-06)	0.077 (0.0103)
2	1220	1.26E-04 (2.20E-05)	0.1542 (0.0268)	2.46E-04 (2.24E-05)	0.3 (0.0274)	6.04E-05 (8.12E-06)	0.0737 (0.0099)
3	1015	1.26E-04 (2.20E-05)	0.1283 (0.0223)	2.46E-04 (2.24E-05)	0.2496 (0.0228)	6.04E-05 (8.12E-06)	0.0613 (0.0082)
4	1195	1.26E-04 (2.20E-05)	0.1511 (0.0263)	2.46E-04 (2.24E-05)	0.2938 (0.0268)	6.04E-05 (8.12E-06)	0.0722 (0.0097)
5	1145	1.26E-04 (2.20E-05)	0.1447 (0.0252)	2.46E-04 (2.24E-05)	0.2815 (0.0257)	6.04E-05 (8.12E-06)	0.0692 (0.0093)
6	880	1.26E-04 (2.20E-05)	0.1112 (0.0193)	2.46E-04 (2.24E-05)	0.2164 (0.0197)	6.04E-05 (8.12E-06)	0.0532 (0.0071)
Average	1121.67	1.26E-04	0.1369	2.46E-04	0.2666	6.04E-05	0.0655
(SD)	(147.57)	(2.20E-05)	(0.0098)	(2.24E-05)	(0.01)	(8.12E-06)	(0.0036)

For 3D-CRT technique, each patient received dose from image verification protocol for seven treatment fields and anterior-posterior plus lateral setup. The image doses from field and setup verification determined for a single protocol were expressed in Gy/MU. Results of measurements are presented in Table 5.17. The imaging dose from verification protocol was the doses in Gy/MU multiplied by MU for seven treatment fields and anterior-posterior plus lateral setup as shown in Table 5.18

Table 5.17 Image doses from field and setup verification for 3D-CRT technique measured in 15 positions with 6 MV photon beam. Data are means (SD).

Organ	Image doses (Gy/MU)		
	Field verification	Setup verification	Total treatment
Outside the image field			
Brain	7.34E-06	6.12E-06	1.35E-05
	(2.15E-07)	(7.57E-07)	(7.87E-07)
Right thyroid	8.17E-06	8.78E-06	1.70E-05
	(1.93E-07)	(4.21E-07)	(4.63E-07)
Left thyroid	7.95E-06	8.45E-06	1.64E-05
	(6.09E-07)	(3.17E-07)	(6.87E-07)
Right lung	1.50E-05	1.76E-05	3.26E-05
	(5.89E-07)	(4.17E-07)	(7.22E-07)
Left lung	1.44E-05	1.60E-05	3.04E-05
	(4.49E-07)	(1.76E-07)	(4.82E-07)
Sternum	1.26E-05	1.61E-05	2.87E-05
	(4.91E-07)	(2.87E-07)	(5.69E-07)
Liver	3.24E-05	3.64E-05	6.88E-05
	(9.90E-07)	(1.01E-06)	(1.41E-06)
Stomach	3.26E-05	3.79E-05	7.05E-05
	(5.57E-07)	(6.23E-07)	(8.36E-07)
Right kidney	8.68E-05	9.27E-05	1.80E-04
	(2.77E-06)	(1.44E-06)	(3.12E-06)
Left kidney	9.14E-05	9.44E-05	1.86E-04
	(2.50E-06)	(1.34E-06)	(2.84E-06)
Inside the image field			
Bladder	0.0058	0.0055	0.0113
	(0.0003)	(0.0002)	(0.0003)
Rectum	0.0047	0.0047	0.0094
	(0.0001)	(0.0003)	(0.0003)
Tumor center	0.0072	0.0069	0.0141
	(0.0002)	(0.0001)	(0.0002)
*Skin dose	0.0024	0.0026	0.0051
	(1.61E-05)	(0.0001)	(0.0001)

Table 5.18 Image doses (Gy) from field and setup verification for 3D-CRT technique with 6 MV photon beam. Data are means (SD).

Organ	Image doses (Gy)		
	Field Verification (7 MU)	Setup verification (14 MU)	Total treatment
Outside the image field			
Brain	5.14E-05	8.57E-05	0.0001
	(1.51E-06)	(1.06E-05)	(1.07E-05)
Right thyroid	5.72E-05	1.23E-04	0.0002
	(1.35E-06)	(5.90E-06)	(6.05E-06)
Left thyroid	5.56E-05	1.18E-04	0.0002
	(4.26E-06)	(4.43E-06)	(6.15E-06)
Right lung	1.05E-04	2.46E-04	0.0004
	(4.13E-06)	(5.84E-06)	(7.15E-06)
Left lung	1.01E-04	2.24E-04	0.0003
	(3.14E-06)	(2.47E-06)	(4E-06)
Sternum	8.80E-05	2.26E-04	0.0003
	(3.43E-06)	(4.01E-06)	(5.28E-06)
Liver	2.27E-04	5.10E-04	0.0007
	(6.93E-06)	(1.41E-05)	(1.57E-05)
Stomach	2.28E-04	5.30E-04	0.0008
	(3.90E-06)	(8.72E-06)	(9.55E-06)
Right kidney	6.07E-04	0.0013	0.0019
	(1.94E-05)	(2.02E-05)	(2.80E-05)
Left kidney	6.40E-04	0.0013	0.0019
	(1.75E-05)	(1.88E-05)	(2.57E-05)
Inside the image field			
Bladder	0.0408	0.0776	0.1184
	(0.0020)	(0.0026)	(0.0033)
Rectum	0.0331	0.0660	0.0991
	(0.0007)	(0.0046)	(0.0047)
Tumor center	0.0504	0.0961	0.1465
	(0.0011)	(0.0015)	(0.0019)
*Skin dose	0.0169	0.0364	0.0533
	(0.0001)	(0.0011)	(0.0011)

In 3D-CRT, each patient received equal imaging doses from field and setup verification protocol. Image doses to PTV, bladder and rectum were 0.1465 Gy, 0.1184 Gy, 0.0991 Gy, respectively (Table 5.18).

5.3.2 Calculation of OED image (OED_{image})

The OED_{image} was calculated using the equation 10. The imaging doses to PTV, bladder and rectum were converted to EQD_2. OED_{image} based on EQD_2 estimates were calculated and are shown in Table 5.19.

Table 5.19 OED_{image} for CK-SBRT and 3D-CRT.

Organ	EQD_2		OED, Gy		$\frac{CK-SBRT}{3D-CRT}*$	P-value*
	CK-SBRT	3D-CRT	CK-SBRT	3D-CRT		
PTV	0.0795 (0.0058)	0.0843 (0.0015)	0.0791 (0.0057)	0.0838 (0.0014)	0.9439 (0.0698)	0.678
Bladder	0.2234 (0.0084)	0.0987 (0.0038)	0.2201 (0.0082)	0.0980 (0.0037)	2.2459 (0.1191)	0.0001
Rectum	0.0547 (0.0030)	0.0826 (0.0033)	0.0545 (0.0030)	0.0821 (0.0032)	0.6638 (0.0448)	0.0004

*Comparison of OED between CK-SBRT and 3D-CRT

OED_{image} for bladder from CK-SBRT technique was significantly greater from 3D-CRT technique whereas OED_{image} of rectum was lower. No significant difference between two treatment plans for OED_{image} of PTV.

5.4 Total organ equivalent dose (OED_T)

Table 5.20-5.22 shows the total organ equivalent dose (OED_T) for PTV, bladder and rectum from CK-SBRT compared with 3D-CRT plans. OED_T for these organs were the summation of the OED_{prim}, $OED_{scatter/leakage}$, and OED_{image}. OED_{prim} (>95%) was a major part of OED_T followed by OED_{image}, while $OED_{scatter/leakage}$ was a small contribution to the OED_T. For the PTV, OED_T from CK-SBRT was 29.06% less than that from 3D-CRT ($p << 0.0001$). In contrast, CK-SBRT induced larger OED to the bladder, i.e. 17.57% ($p = 0.0005$), whereas no significant difference in OEDs could be observed for the rectum by both techniques.

Figures 5.1-5.3 compare OEDs for primary beam, scatter/leakage and imaging dose generated by CK-SBRT and 3D-CRT to the PTV, bladder and rectum.

Table 5.20 OED_T for PTV from CK-SBRT and 3D-CRT.

Patient code	CK-SBRT							3D-CRT							% Diff*
	OEDprim		OEDscatter/leakage		OEDimage		OED_T	OEDprim		OEDscatter/leakage		OEDimage		OED_T	
	Gy	% of total	Gy	% of total	Gy	% of total	Gy	Gy	% of total	Gy	% of total	Gy	% of total	Gy	
1	1.746	94.93	2.11E-04	0.0115	0.0931	5.06	1.8393	2.5582	96.82	1.67E-04	0.0063	0.0838	3.17	2.6422	-30.3863
2	1.7581	95.17	1.35E-04	0.0073	0.0891	4.82	1.8473	2.5397	96.80	7.62E-05	0.0029	0.0838	3.19	2.6236	-29.5871
3	1.6671	95.74	1.55E-04	0.0089	0.074	4.25	1.7413	2.4239	96.65	1.18E-04	0.0047	0.0838	3.34	2.5078	-30.5669
4	1.8586	95.51	1.15E-04	0.0059	0.0872	4.48	1.9459	2.4712	96.72	9.98E-05	0.0039	0.0838	3.28	2.5551	-23.8419
5	1.7627	95.46	1.76E-04	0.0095	0.0836	4.53	1.8465	2.5132	96.77	1.06E-04	0.0041	0.0838	3.23	2.5971	-28.9026
6	1.7126	96.38	1.23E-04	0.0069	0.0642	3.61	1.7769	2.4933	96.74	8.97E-05	0.0035	0.0838	3.25	2.5772	-31.0519
Average	1.7509	95.53	1.53E-04	0.0083	0.0819	4.46	1.8329	2.4999	96.75	1.09E-04	0.0042	0.0838	3.24	2.5838	-29.0561
(SD)	(0.0637)	(0.5)	(3.62E-05)	(0.002)	(0.0108)	(0.5)	(0.0703)	(0.0486)	(0.06)	(3.16E-05)	(0.0012)	(0)	(0.06)	(0.0486)	(2.6657)

$$* \% \text{ Diff} = \left(\frac{\text{OED}_{\text{CK-SBRT}} - \text{OED}_{\text{3D-CRT}}}{\text{OED}_{\text{3D-CRT}}}\right) \times 100$$

Table 5.21 OED_T for bladder from CK-SBRT and 3D-CRT.

Patient code	CK-SBRT							3D-CRT							% Diff*
	OEDprim		OEDscatter/leakage		OEDimage		OED_T	OEDprim		OEDscatter/leakage		OEDimage		OED_T	
	Gy	% of total	Gy	% of total	Gy	% of total	Gy	Gy	% of total	Gy	% of total	Gy	% of total	Gy	
1	6.6274	96.25	3.58E-04	0.0052	0.2581	3.75	6.8859	5.8269	98.34	2.04E-04	0.0034	0.098	1.65	5.9251	16.2150
2	6.1456	96.13	1.99E-04	0.0031	0.2471	3.87	6.3929	5.7695	98.33	8.79E-05	0.0015	0.098	1.67	5.8676	8.9528
3	5.8643	96.60	3.01E-04	0.0050	0.206	3.39	6.0706	5.44	98.23	1.80E-04	0.0033	0.098	1.77	5.5382	9.6136
4	6.1408	96.20	2.20E-04	0.0034	0.2421	3.79	6.3831	5.2322	98.16	1.37E-04	0.0026	0.098	1.84	5.3303	19.7508
5	5.9347	96.23	2.96E-04	0.0048	0.2321	3.76	6.1671	4.9603	98.06	1.44E-04	0.0028	0.098	1.94	5.0584	21.9169
6	4.4788	96.16	2.92E-04	0.0063	0.1788	3.84	4.6579	3.5135	97.28	1.58E-04	0.0044	0.098	2.71	3.6117	28.9682
Average	5.8653	96.26	2.78E-04	0.0046	0.2274	3.73	6.0929	5.1237	98.07	1.52E-04	0.0030	0.098	1.93	5.2219	17.5695
(SD)	(0.7297)	(0.17)	(5.84E-05)	(0.0012)	(0.0296)	(0.17)	(0.7574)	(0.8536)	(0.4)	(3.98E-05)	(0.001)	(0)	(0.4)	(0.8536)	(7.6546)

$$* \%\ \text{Diff} = \left(\frac{\text{OED}_{\text{CK-SBRT}} - \text{OED}_{\text{3D-CRT}}}{\text{OED}_{\text{3D-CRT}}}\right) \times 100$$

Table 5.22 OED_T for rectum from CK-SBRT and 3D-CRT.

Patient code	CK-SBRT							3D-CRT							% Diff*
	OEDprim		OEDscatter/leakage		OEDimage		OED_T	OEDprim		OEDscatter/leakage		OEDimage		OED_T	
	Gy	% of total	Gy	% of total	Gy	% of total	Gy	Gy	% of total	Gy	% of total	Gy	% of total	Gy	
1	6.1139	98.96	1.55E-04	0.0025	0.064	1.04	6.1781	5.9352	98.63	8.85E-05	0.0015	0.0821	1.36	6.0174	2.6700
2	5.0652	98.80	4.38E-04	0.0085	0.0613	1.20	5.1269	5.5707	98.54	1.94E-04	0.0034	0.0821	1.45	5.6530	-9.3058
3	5.9135	99.14	1.27E-04	0.0021	0.051	0.86	5.9646	5.837	98.61	7.58E-05	0.0013	0.0821	1.39	5.9192	0.7679
4	5.0837	98.83	1.33E-04	0.0026	0.06	1.17	5.1438	4.6262	98.25	8.28E-05	0.0018	0.0821	1.74	4.7084	9.2484
5	6.2414	99.08	1.81E-04	0.0029	0.0575	0.91	6.2991	5.6415	98.56	8.82E-05	0.0015	0.0821	1.43	5.7237	10.0528
6	4.8629	99.10	7.92E-05	0.0016	0.0442	0.90	4.9072	4.5275	98.22	4.29E-05	0.0009	0.0821	1.78	4.6096	6.4546
Average	5.5468	98.99	1.86E-04	0.0034	0.0563	1.01	5.6033	5.3564	98.47	9.54E-05	0.0017	0.0821	1.53	5.4385	3.3147
(SD)	(0.6087)	(0.15)	(1.28E-04)	(0.0026)	(0.0074)	(0.14)	(0.6112)	(0.6186)	(0.19)	(5.12E-05)	(0.0009)	(0)	(0.19)	(0.6186)	(7.1645)

$$* \%\ \text{Diff} = \left(\frac{\text{OED}_{\text{CK-SBRT}} - \text{OED}_{\text{3D-CRT}}}{\text{OED}_{\text{3D-CRT}}}\right) \times 100$$

Table 5.23 shows the paired t-test for the difference between CK-SBRT and 3D-CRT plan. Compared with 3D-CRT, CK-SBRT was significantly lower OED_T in PTV but higher OED_T in bladder. For OED_T of rectum was not significant difference from two treatment plans.

Table 5.23 Comparison between OED_T's from CK-SBRT and 3D-CRT.

Organ	CK-SBRT $\bar{X}$(SD), Gy	3D-CRT $\bar{X}$(SD), Gy	$\frac{CK-SBRT}{3D-CRT}$	P-value
PTV	1.8329 (0.0703)	2.5838 (0.0486)	0.7094 (0.0303)	<< 0.0001
Bladder	6.0929 (0.7574)	5.2219 (0.8536)	1.1668 (0.2396)	0.0005
Rectum	5.6033 (0.6112)	5.4385 (0.6186)	1.0303 (0.1624)	0.346

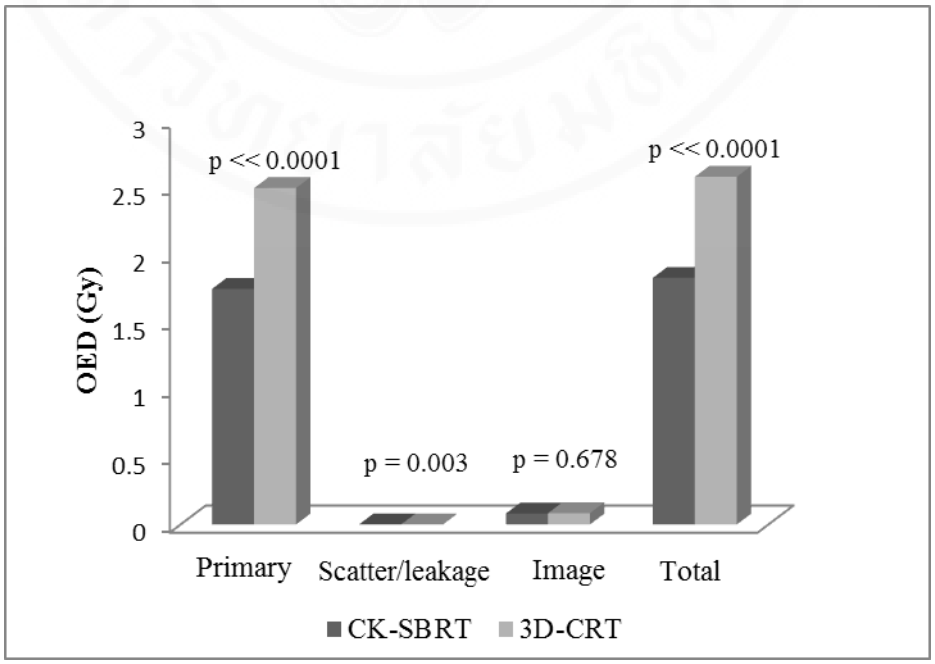

Figure 5.1 The average OEDs for primary beam, scatter/leakage radiation, imaging and total OED for PTV from CK-SBRT and 3D-CRT.

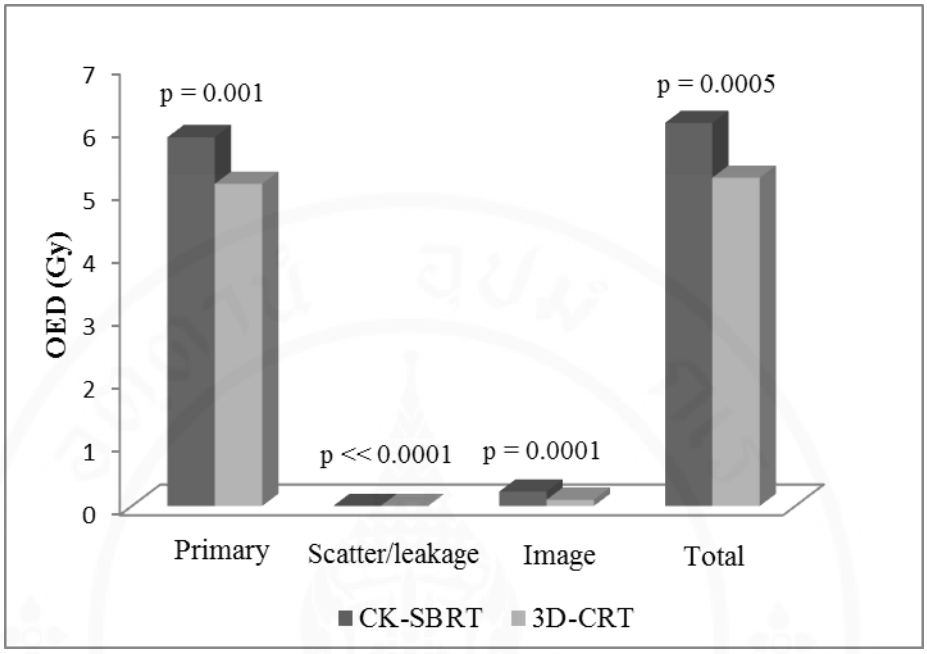

Figure 5.2 The average OEDs for primary beam, scatter/leakage radiation, imaging and total OED for bladder from CK-SBRT and 3D-CRT.

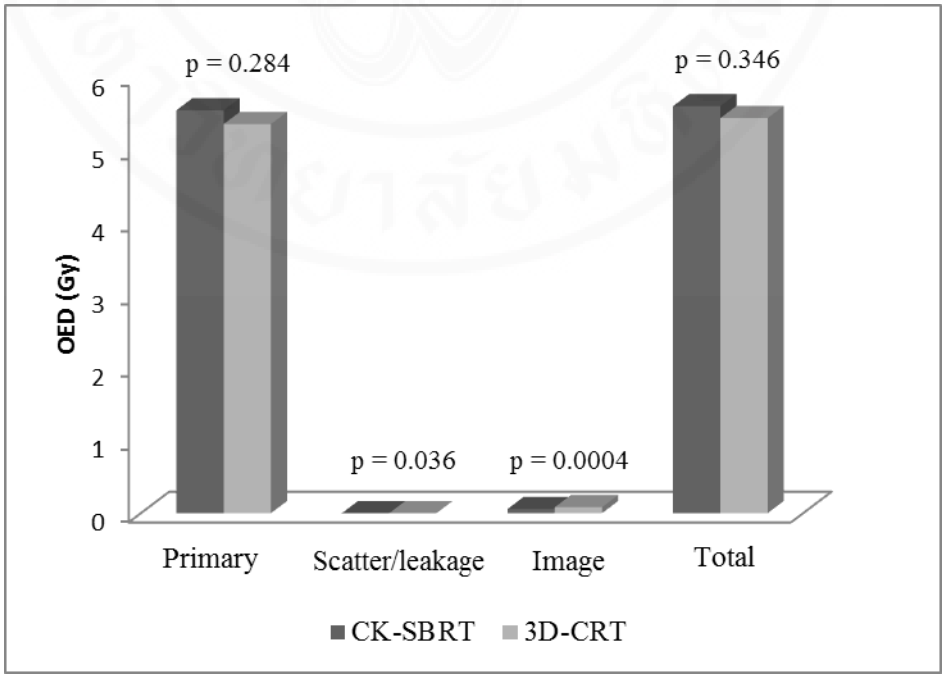

Figure 5.3 The average OEDs for primary beam, scatter/leakage radiation, imaging and total OED for rectum from CK-SBRT and 3D-CRT.

CHAPTER VI
DISCUSSION

The risk of secondary malignancies after radiotherapy is a subject of concern for modern conformal radiotherapy techniques. Precise dose targeting will allow dose escalation to achieve a better cure rate and long-term survivorship. The use of highly conformal SBRT in the treatment of prostate cancer (PCa) bases on the capability in accurate delivery (with the aid of an organ motion tracking system) of highly conformal tumor dose and the use of ablative dose fractions for effective killing of the late responding PCa ($\alpha/\beta = 2.7$ Gy) [26, 27]. Theoretical prediction of radiation-induced secondary malignancies (RISM) after fractionated radiotherapy using the linear-quadratic formular suggests that hypofractionated radiotherapy has the potential for secondary cancer reduction. Of particular interest is the more pronounced reduction on risks of sarcoma than carcinoma risks [41].

Like many other modern radiotherapeutic techniques, CK-SBRT treatment in comparing to the conventional 3D-CRT involves larger number of small fields to achieve precise tumor targeting resulting larger volume of normal tissues being exposed to small radiation doses. By this token, better local tumor control and reduced normal tissue complications can be expected for CK-SBRT. Despite this therapeutic efficacy, there is a concern that CK-SBRT in relative to 3D-CRT might be associated with an increase in risk of RISM for many reasons, namely: the spreading of low doses and hence carcinogenic effect to large volume of normal tissues, larger monitor unit (MU) requirement contributing larger total body doses from collimator scatter and machine leakage radiations, concomitant imaging doses from tumor motion tracking [15, 17, 31].

In this study, the impact of CK-SBRT on RISM compared to 3D-CRT was evaluated for the planning target volume (PTV) and organs at beam borders including bladder and rectum. Since RISM is commonly observed inside or close to the treatment volume [8], RISM was assessed by employing the organ equivalent dose

(OED), a dosimetric index of RISM developed by Schneider et al [25]. OED projecting in-field risk was calculated by the linear-exponential model (LE) [23] and out-of-field risk by the linear-plateau model (LP) [24]. All physical doses were normalized to an equivalent dose in 2 Gy fractions (EQD_2) by applying linear-quadratic model (LQ) model. The LQ model is suggested to be a reliable and mechanically plausible model for designing protocol in the dose per fraction range from 2 to 10 Gy [42]. A loss in accuracy can be expected above 10 Gy [42]. However, animal studies demonstrated the model validity for designing clinical trials with fraction doses of up to 15-18 Gy [42]. In evaluation of the primary beam effect on PTV where similar dose distributions were observed for CK-SBRT and 3D-CRT plans, OED_{prim} from CK-SBRT was 1.43 times less than OED_{prim} from 3D-CRT ($p << 0.0001$). The difference might be due to difference in size of dose per fraction, i.e. ablative dose fractions used in CK-SBRT treatment against the conventional dose fractions in 3D-CRT. The effectiveness of large dose fraction in better cell killing than conventional dose fraction may help elimination of radiation-induced mutant cells hence reducing the risk of RISM [14].

For non-target organs within the planning CT volume, OED_{prim} was dependent on dose distribution specified by the differential dose volume histogram. For bladder, the ratio between $EQD_{2\ (out\ PTV)}$ to $EQD_{2\ (in\ PTV)}$ was 29.9:1 for CK-SBRT in contrast to 6.5:1 for 3D-CRT (Table 5.2). The greater OED_{prim} obtained for CK-SBRT plan (i.e. 1.14 times larger than 3D-CRT) was the result of larger percentage of bladder volume being exposed to low doses spread by CK-SBRT technique. Risk of RISM at low doses was defined by the linear portion of the LP model. In contrast, more bladder volumes, by 3D-CRT plan, were included in the treatment field where RISM was decreased by increasing dose as defined by the downward part of the LE model. For rectum, differences in dose distributions for these plans followed the same trends as in the bladder. But OEDs from these plans did not differ significantly. By inspecting the dose distribution between out-of-field and in-field, the magnitude of difference in dose distribution observed for CK-SBRT and 3D-CRT was less than what recognized for the bladder (Table 5.3).

Longer beam-on time, larger number of MUs required for CK-SBRT generated a 2.1 fold higher scatter/leakage dose than 3D-CRT. The scatter/leakage

dose is associated with the amount of MUs in a linear function [43]. In terms of OED, longer beam-on time operated for CK-SBRT, on average, caused a 1.6 fold increase in scatter/leakage OED to all organs under study.

Modern radiotherapeutic units employ radiographic imaging for different purposes and importing different doses to patients. CK-SBRT imaging serves to guide tumor targeting by tracking organ motion while 3D-CRT in this study employs imaging to verify field and setup procedures. Imaging doses to region/organs in this study were observed to vary according to the number of images taken for the whole treatment. For PTV, estimates of OED_{image} for CK-SBRT and 3D-CRT were comparable. In bladder, the OED_{image} for CK-SBRT was 2.2 folds greater than 3D-CRT, while in rectum the OED_{image} was only 66% of OED_{image} from 3D-CRT.

In overall, OED_{prim} was the major component of OED_T (with > 95% contribution), followed by OED_{image} (between 1-4% contribution) and $OED_{scatter/leakage}$ (< 1% contribution). Thereby, OED_T for PTV from CK-SBRT plan was 1.4 folds less than that from 3D-CRT plan. In bladder, CK-SBRT treatment caused a 1.2 fold increase in OED as compared to 3D-CRT. In rectum, estimates of OED_T for both treatment plans were comparable.

OED concept proposed by Schneider et al [25] is an index used for assessing the carcinogenic impact of radiotherapy. OED is proportional to absolute risk estimate. In converting OED into an absolute risk estimate, excess absolute risk (EAR), requires two additional parameter: β, the initial slope in the unit of excess cases per 10,000 person Gy and μ, the population dependent variables specified for age at exposure and age attain [44, 45]. Data used for estimation of β and μ are the combination of the Japanese A-bomb survivor data and the secondary cancer data of Hodgkin's patients from the Western population. Although a risk transfer between Japanese and Western populations had been performed. It is advised by Schneider et al [44, 45] that EAR estimates thus obtained must be viewed with care, since the errors involved are large. For the interest to know whether a treatment modality is better than the standard treatment modality with respect to cancer induction in one patient, evaluation of the risk ratio based on OED ratio is considered sufficient.

Despite the fact that larger MUs employed by modern radiotherapeutic techniques such as CK-SBRT cause the significant larger scatter/leakage OED in

comparing to 3D-CRT, but the risk is negligible small. In addition, the doses of imaging procedures during the radiotherapy process, which increase dose in patient. However, the increase in risk is tiny compared to the benefit of treatment.

CHAPTER VII
CONCLUSIONS

1. Primary beam component, OED for PTV from CK-SBRT plan was 1.43 times less ($p << 0.0001$), while the OED for bladder was 1.14 times ($p = 0.001$) more than those of 3D-CRT. For OED of rectum was not significant difference between the two treatment plans ($p = 0.284$).

2. For scatter/leakage component, The OED for PTV, bladder and rectum from CK-SBRT plan was significantly greater than from 3D-CRT plan ($p \leq 0.036$).

3. Imaging doses component, OED for bladder from CK-SBRT technique was significantly greater from 3D-CRT technique ($p = 0.0001$) whereas OED of rectum was lower ($p = 0.0004$). No significant difference between two treatment techniques was observed for OED of PTV.

4. Overall, total OEDs for PTV generated by CK-SBRT (1.83 Gy) was 1.41 times less than that (2.58 Gy) of 3D-CRT ($p << 0.0001$). In contrast, total OEDs of bladder generated by CK-SBRT (6.09 Gy) was 1.17 times greater than that (5.22 Gy) of 3D-CRT ($p = 0.0005$). For rectum, No significant difference between two treatment plans ($p = 0.346$).

5. Primary OED is a major part of total OEDs (> 95% of total OEDs), followed by image OED and scatter/leakage OED.

REFERENCES

1. Center MM, Jemal A, Lortet-Tieulent J, Ward E, Ferlay J, Brawley O, Bray F. International variation in prostate cancer incidence and mortality rates. European Urology. 2012;61:1079-92.
2. Platz EA, Giovannucci E. Prostate cancer. In: Schottenfeld D, Fraumeni JF, editors. Cancer epidemiology and prevention. New York, NY: Oxford University Press; 2006. p. 1128-50.
3. Jani AB, Hellman S. Early prostate cancer: clinical decision-making. Lancet. 2003;361:1045-53.
4. Cooperberg MR, Moul JW, Carroll PR. The changing face of prostate cancer. J Clin Oncol. 2005;23:8146-51.
5. Speight JL, Roach M III. Radiotherapy in the management of clinically localized prostate cancer: evolving standards , consensus, controversies and new directions. J Clin Oncol. 2005;23:8176-85.
6. Muller AC, Ganswindt U, Bamberg M, Belka C. Risk of second malignancies after prostate irradiation?. Strahlenther Onkol. 2007;183:605-9.
7. Quilty PM, Kerr GR. Bladder cancer following low or high dose pelvic irradiation. Clin Radiol. 1987;38:583-5.
8. Hall PF. Cancer risks after medical radiation. Med Oncol Tumor Pharmacother. 1991;8:141-5.
9. Suit H, Goldberg S, Niemierko A, et al. Secondary carcinogenesis in patients treated with radiation: a review of data on radiation induced cancers in human, non-human primate, canine and rodent subjects. Radiat Res. 2007;167:12-42.
10. Bostrom PJ, Soloway MS. Secondary cancer after radiotherapy for prostate cancer: should we be more aware of the risk?. European Urology. 2007;52:973-82

11. Pickles T, Phillips N. The risk of second malignancy in men with prostate cancer treated with or without radiation in British Columbia, 1984-2000. Radiat Oncol. 2002;65:145-51.
12. Brenner DJ, Curtis RE, Hall EJ, Ron E. Second malignancies in prostate carcinoma patients after radiotherapy compared with surgery. Cancer. 2000;88:398-406.
13. Moon K, Stukenborg GJ, Keim J, Theodorescu D. Cancer incidence after localized therapy for prostate cancer. Cancer. 2006;107:991-8.
14. Hall EJ, Wuu CS. Radiation-induced second cancers: the impact of 3D-CRT and IMRT. Int J Radiat Oncol Biol Phys. 2003;56:83-88.
15. Xu XG, Bednarz B, Paganetti H. A review of dosimetry studies on external-beam radiation treatment with respect to second cancer induction. Phys Med Biol. 2008;53:193-241.
16. Diallo I, Haddy N, Adjadj E, Samand A, Quiniou E, Chavaudra J, Alziar I, Perret N, Guerin S, Lefkopoulos D, de Vathaire F. Frequency distribution of second solid cancer locations in relation to the irradiated volume among 115 patients treated for childhood cancer. Int J Radiat Oncol Biol Phys. 2009;74(3):876-883.
17. Murray L, et al. Second primary cancers after radiation for prostate cancer: a review of data from planning studies. Radiation Oncology. 2013;8:1-12
18. Huang J, Kestin LL, Ye H, Wallace M, Martinez AA, Vicini FA. Analysis of second malignancies after modern radiotherapy versus prostatectomy for localized prostate cancer. Radiotherapy and Oncology. 2011;98:81-86.
19. Zelefsky MJ, Housman DM, Pei X, Alicikus Z, Magsanoc JM, Dauer LT, St Germain J, Yamada Y, Kollmeier M, Cox B, Zhang Z. Incidence of secondary cancer development after high-dose intensity-modulated radiotherapy and image-guided brachytherapy for the treatment of localized prostate cancer. Int J Radiat Oncol Biol Phys. 2012;83:953-59.
20. Zelefsky MJ, Pei X, Teslova T, Kuk D, Magsanoc JM, Kollmeier M, Cox B, Zhang Z. Secondary cancers after intensity-modulated radiotherapy, brachytherapy and radical prostatectomy for the treatment of prostate

cancer: incidence and cause-specific survival outcomes according to the initial treatment intervention. BJU Int. 2012;110:1696-1701.

21. Shuryak I, Sachs RK, Hlatky L, Little MP, Hahnfeldt P, Brenner DJ. Radiation-induced leukemia at doses relevant to radiation therapy: modeling mechanisms and estimating risks. J Nat Cancer Inst. 2006;98(24):1794-1806.
22. Sachs RK, Brenner DJ. Solid tumor risks after high doses of ionizing radiation. PNAS. 2005;102(37):13040-45.
23. Schneider U, Zwahlen D, Ross D, Kaser-Hotz B. Estimation of radiation-induced cancer from three-dimensional dose distributions: concept of organ equivalent dose. Int J Radiat Oncol Biol Phys. 2005;61(5):1510-15.
24. Schneider U, Kaser-Hotz B. Radiation risk estimates after radiotherapy: application of the organ equivalents dose concept to plateau dose-response relationships. Radiat Environ Biophys. 2005;44:235-239.
25. Schneider U, Walsh L. Cancer risk estimates from the combined Japanese A-bomb and Hodgkin cohorts for doses relevant to radiotherapy. Radiat Environ Biophys. 2008;47:253-263.
26. Buyyounouski MK, Price RA Jr, Harris EE, et al. Stereotactic body radiotherapy for primary management of early-stage, low- to intermediate-risk prostate cancer: report of the American society for therapeutic radiology and oncology emerging technology committee. Int J Radiat Oncol Biol Phys. 2010;76(5):1297-1304.
27. Oliveira SM, Teixeira NJ, Fernandes L, What do we know about the α/β for prostate cancer?. Med Phys. 2012;39(6):3189-3201.
28. Ruben JD, Davis S, Evans C, Jones P, Gagliardi F, Haynes M, Hunter A. The effect of intensity-modulated radiotherapy on radiation-induced second malignancies. Int J Radiat Oncol Biol Phys. 2008;70:1530-36.
29. Spiess H, Mays CW. Bone cancers induced by 224Ra (Th X) in children and adults. Health Phys. 1970;19(6):713-29.
30. Sigurdson AJ, Ronckers CM, Mertens AC, Stovall M, Smith SA, Liu Y, Berkow RL, Hammond S, Neglia JP, Meadows AT, Sklar CA, Robison LL, Inskip PD. Primary thyroid cancer after a first tumour in childhood (the

Childhood Cancer Survivor Study): a nested case-control study. Lancet. 2005;365:2014-23.

31. Hall EJ, Phil D. Intensity-modulated radiation therapy, protons, and the risk of second cancers. Int J Radiat Oncol Biol Phys. 2006;65(1):1-7.
32. Schneider U, Lomax A, Pemler P, Besserer J, Ross D, Lombriser N, Kaser-Hotz B. The impact of IMRT and proton radiotherapy on secondary cancer incidence. Strahlenther Onkol. 2006;182:647-52.
33. McKinlay AF. Thermoluminescence dosimetry, Medical physics handbook 5. Bristol: Adam Hilger; 1981.
34. LiF:Mg,Cu,P Physical data and constants [database on the internet]. Available from: http://cdf-radmon.fnal.gov/dosimetry/MCP_Physical_Constants.pdf.
35. Timmerman RD. An overview of hypofractionation and introduction to this issue of seminars in radiation oncology. Semin Radiat Oncol. 2008;18(4):215-22.
36. Joiner M, van der Kogel A. Basic clinical radiobiology. Fourth edition. London: Hodder-Arnold Publishing; 2009.
37. Borras C, Bares JP, Rudder D, Amer A, Millan F, Abuchaibe O. Clinical effects in a cohort of cancer patients overexposed during external beam pelvic radiotherapy. Int J Radiat Oncol Biol Phys. 2004;59(2):538-50.
38. International Commission on Radiological Protection (ICRP). Report on the Task Group on Reference man, ICRP Publication 23. Oxford: Pergamon Press; 1975.
39. Zar JH. Two-sample hypotheses. Biostatistical analysis. 4th ed: Prentice Hall; 1999. p. 122-7.
40. Sharma SD, Upreti RR, Laskar S, Tambe CM, Deshpande DD, Shrivastava SK, Dinshaw KA. Estimation of risk of radiation-induced carcinogenesis in adolescents with nasopharyngeal cancer treated using sliding window IMRT. Radiother Oncol. 2008;86:177-81.
41. Schneider U, Besserer J, Mack A. Hypofractionated radiotherapy has the potential for second cancer reduction. Theor Biol Med Model. 2010;7:4.

42. Brenner DJ. The linear-quadratic model is an appropriate methodology for determining isoeffective doses at large doses per fraction. Semin Radiat Oncol. 2008;18:234-39.

43. Kry SF, Salehpour M, Followill DS, Stovall M, Kuban DA, White RA, Rosen II. The calculated risk of fatal secondary malignancies from intensity-modulated radiation therapy. Int J Radiat Oncol Biol Phys. 2005;62(4):1195-1203.

44. Schneider U. Modeling the risk of secondary malignancies after radiotherapy. Genes. 2011;2:1033-49.

45. Schneider U, Sumila M, Robotka J. Site-specific dose-response relationships for cancer induction from the combined Japanese A-bomb and Hodgkin cohorts for doses relevant to radiotherapy. Theor Biol Med Model. 2011;8:27.

46. Harshaw Bicron. Automatic TLD reader user's manual, Saint-Gobain/Norton Industrial Ceramics Co., Ohio, 1993.

APPENDIX

1. TLD-700 preparation

1.1 TLD-700 calibration

The processes of TLD-700 calibration were:

i) Anneal all 197 rods of TLD-700 with annealing program at 400 ^{o}C for 1 hour and 100 ^{o}C for 2 hours to eliminate the residual signal in the TLDs.

ii) TLDs were placed in a perspex phantom and irradiated by the cobalt-60 machine to achieve a dose of 0.5 Gy. The exposed TLDs were heated with preheating program at 100 ^{o}C for 10 minutes to eliminate off-peak noise before reading the nanocoulomb (nC) by the TLD reader.

iii) Determine the element correction coefficient (ECC_i) for each TLD which described by equation 11, and select 15 of all TLDs which had the ECC_i value closest to 1 used for the TLD calibrations.

$$ECC_i = \frac{\bar{Q}}{Q_i} \tag{11}$$

Where $\bar{Q}$ is the average charge of all TLD rods and Q_i is the individual reading of each TLD.

iv) Anneal and irradiate the selected TLDs from (iii) with a dose of 0.5 Gy from the cobalt-60 machine which repeat step (i) and (ii). The corrected charge integral (Q_{ci}) of these group was calculated by equation 12.

$$Q_{ci} = Q_i \times ECC_i \tag{12}$$

v) The average value of the Q_{ci} from (iv) was used for the calculation of the reader calibration factor (RCF) for the whole set of TLDs which defined by equation 13.

$$RCF = \frac{\overline{Q_c}}{D} \tag{13}$$

Where $\overline{Q_c}$ is the average value of the Q_{ci}, and D is the known dose in gray (Gy) which was 0.5 Gy.

vi) Anneal and irradiate the rest of TLDs (182 rods) with a dose of 0.5 Gy from the cobalt-60 machine which repeat step (i) and (ii). Calculated the individual element correction coefficient (ECC_{ci}) according to equation 14.

$$ECC_{ci} = \frac{RCF \times D}{Q_i} \quad (14)$$

Where D is known dose (0.5 Gy) which irradiated to TLDs and Q_i is the individual reading of each TLD

vii) The ECC_{ci} value for each TLD was used to determine an unknown dose (D_u) according to equation 15.

$$D_u = \frac{Qi \times ECC_{ci}}{RCF} \quad (15)$$

Where Q_i is the individual reading of each TLD from measurement in Rando phantom.

In this study, the ECCi value of 197 rods ranged from 0.9059 to 1.2477. These variations were within the acceptable range as recommended in manual (0.7-1.3) [46]. The reader calibration factor (RCF) for the whole set of TLDs was 4560.89708 nC/Gy with the ECC_{ci} value for each TLD used to convert the reading in nC of each TLD to absorbed dose. The ECCi and ECC_{ci} value were shown in Tables A.1-A.2

Table A.1 The element correction coefficient (ECC_i) value for TLD-700.

TLD No.	ECC_i	TLD No.	ECC_i	TLD No.	ECC_i	TLD No.	ECC_i
1*	0.9982	26	0.9729	51	0.9495	76	0.9590
2	0.9805	27	0.9490	52	0.9644	77	1.1596
3	0.9687	28	1.2445	53	0.9651	78	0.9521
4	0.9430	29	0.9504	54	0.9623	79	0.9537
5	0.9635	30	0.9669	55	1.1291	80	0.9444
6	0.9489	31	1.2022	56	1.2116	81	0.9510
7	1.1962	32	0.9545	57	1.1868	82*	1.0059
8	0.9478	33	0.9604	58	0.9391	83*	0.9975
9	0.9631	34	0.9672	59*	0.9919	84*	0.9925
10	0.9410	35*	0.9948	60	0.9863	85*	1.0078
11	0.9542	36	0.9727	61	0.9867	86	1.2279
12*	0.9919	37	0.9417	62	0.9655	87	0.9615
13*	0.9908	38	0.9725	63	0.9627	88	1.1826
14	0.9515	39	0.9354	64	1.1756	89	0.9685
15	1.1599	40	0.9714	65	1.1619	90	0.9362
16	0.9640	41	0.9578	66	0.9578	91	0.9408
17	0.9861	42	0.9568	67	0.9338	92	0.9413
18	0.9267	43	0.9404	68	1.2067	93	0.9589
19	0.9483	44	0.9522	69	0.9402	94	1.0403
20	0.9313	45	0.9634	70	0.9594	95	1.0235
21	0.9486	46	0.9640	71	1.0117	96*	0.9902
22	0.9350	47	0.9764	72	0.9754	97	1.2316
23	1.1574	48	1.2403	73	0.9534	98	0.9599
24*	1.0095	49	1.2377	74	0.9803	99	0.9528
25	0.9792	50	1.2477	75	0.9531	100	0.9294

* The TLDs selected for calibration.

Table A.1 The element correction coefficient (ECC_i) value for TLD-700 (cont.).

TLD No.	ECC_i	TLD No.	ECC_i	TLD No.	ECC_i	TLD No.	ECC_i
101	0.9585	126	0.9428	151	0.9365	176	0.9647
102	0.9444	127	0.9488	152	1.1930	177	0.9631
103	0.9567	128	0.9495	153	1.1632	178	0.9507
104	0.9665	129	0.9495	154	1.1736	179	0.9245
105	0.9673	130	1.1982	155	0.9452	180	0.9277
106*	1.0085	131	0.9468	156	1.2038	181	1.2346
107	0.9770	132	1.1952	157	1.1440	182	0.9279
108	0.9594	133	1.2134	158	0.9277	183	1.2022
109	0.9407	134	1.1592	159	0.9071	184	0.9568
110	0.9539	135	0.9389	160	0.9540	185	0.9515
111	0.9459	136	0.9527	161	0.9295	186	1.1987
112	1.2141	137	0.9404	162	0.9655	187*	0.9893
113	0.9541	138	0.9523	163	0.9377	188*	0.9995
114	0.9425	139	0.9686	164*	1.0028	189	0.9685
115	0.9490	140	0.9600	165	0.9838	190	0.9402
116	0.9741	141	0.9620	166	0.9344	191	0.9306
117	0.9757	142	0.9679	167	0.9460	192	0.9232
118	0.9810	143	0.9494	168	0.9380	193	1.1827
119	0.9595	144	0.9662	169	0.9179	194	0.9844
120	0.9620	145	1.2334	170	0.9274	195	0.9463
121	0.9377	146	0.9573	171	0.9389	196	0.9594
122	0.9396	147	0.9254	172	0.9472	197	0.9606
123	0.9386	148	0.9059	173	0.9489		
124	1.1728	149	0.9249	174	1.1997		
125	0.9556	150	0.9190	175	0.9750		

* The TLDs selected for calibration.

Table A.2 The individual element correction coefficient (ECC_{ci}) for TLD-700.

TLD No.	ECC_{ci}	TLD No.	ECC_{ci}	TLD No.	ECC_{ci}	TLD No.	ECC_{ci}
1*	1.0024	26	0.9835	51	0.9857	76	0.9896
2	0.9890	27	0.9729	52	0.9712	77	1.2009
3	0.9911	28	1.2796	53	1.0073	78	0.9815
4	0.9935	29	0.9736	54	0.9875	79	0.9905
5	1.0069	30	0.9680	55	1.1636	80	0.9474
6	0.9752	31	1.2899	56	1.2452	81	0.9880
7	1.2682	32	0.9811	57	1.2324	82*	0.9817
8	0.9950	33	0.9681	58	0.9684	83*	1.0141
9	0.9729	34	0.9720	59*	0.9843	84*	0.9935
10	0.9795	35*	0.9767	60	0.9859	85*	1.0016
11	1.0031	36	0.9800	61	0.9880	86	1.3079
12*	0.9827	37	0.9807	62	1.0067	87	0.9891
13*	0.9881	38	0.9901	63	0.9820	88	1.2189
14	0.9761	39	0.9920	64	1.2223	89	0.9719
15	1.2026	40	0.9859	65	1.2157	90	0.9409
16	0.9807	41	0.9556	66	0.9866	91	0.9358
17	0.9890	42	0.9767	67	0.9683	92	0.9473
18	0.9776	43	0.9858	68	1.2258	93	0.9598
19	0.9795	44	0.9731	69	0.9437	94	1.0375
20	0.9780	45	0.9674	70	0.9613	95	1.0375
21	0.9858	46	0.9875	71	1.0326	96*	1.0058
22	0.9742	47	0.9977	72	0.9722	97	1.2931
23	1.2294	48	1.2771	73	0.9783	98	0.9703
24*	1.0111	49	1.2969	74	0.9922	99	0.9723
25	0.9857	50	1.2952	75	0.9702	100	0.9522

* The TLDs selected for calibration.

Table A.2 The individual element correction coefficient (ECC_{ci}) for TLD-700 (cont.).

TLD No.	ECC_{ci}	TLD No.	ECC_{ci}	TLD No.	ECC_{ci}	TLD No.	ECC_{ci}
101	0.9738	126	1.0046	151	0.9657	176	0.9964
102	0.9841	127	0.9854	152	1.2480	177	0.9771
103	0.9670	128	0.9811	153	1.1962	178	0.9805
104	0.9943	129	0.9957	154	1.2634	179	0.9445
105	0.9722	130	1.2374	155	0.9692	180	0.9571
106*	1.0204	131	0.9604	156	1.2597	181	1.2936
107	1.0061	132	1.2766	157	1.1820	182	0.9572
108	0.9825	133	1.3090	158	0.9555	183	1.2598
109	0.9869	134	1.2143	159	0.9411	184	0.9431
110	0.9855	135	0.9662	160	1.0098	185	0.9803
111	0.9592	136	0.9864	161	0.9730	186	1.2494
112	1.2609	137	0.9871	162	1.0013	187*	1.0034
113	0.9818	138	0.9818	163	0.9759	188*	1.0036
114	0.9675	139	1.0106	164*	1.0037	189	1.0255
115	0.9989	140	1.0023	165	0.9765	190	0.9832
116	0.9831	141	0.9920	166	0.9923	191	0.9468
117	0.9872	142	0.9718	167	0.9896	192	0.9655
118	0.9962	143	0.9709	168	0.9798	193	1.2286
119	0.9908	144	0.9836	169	0.9280	194	0.9862
120	0.9690	145	1.2908	170	0.9421	195	0.9720
121	0.9631	146	0.9802	171	0.9554	196	0.9892
122	0.9790	147	0.9548	172	0.9625	197	0.9963
123	0.9762	148	0.9255	173	0.9699		
124	1.2151	149	0.9753	174	1.2375		
125	0.9907	150	0.9526	175	0.9812		

* The TLDs selected for calibration.

1.2 Linearity test of TLD-700

The linearity of 197 rods were evaluated by irradiate with dose of the cobalt-60 machine for 0.05, 0.1, 0.25, 0.5 and 1 Gy, respectively. The readings of all TLDs from each dose were converted into the unit of dose. The average doses obtained from TLDs were plotted as a linear function of the irradiated values. In this study demonstrated a linear relation with a R^2 of 0.9999 which shown in Figure A.1

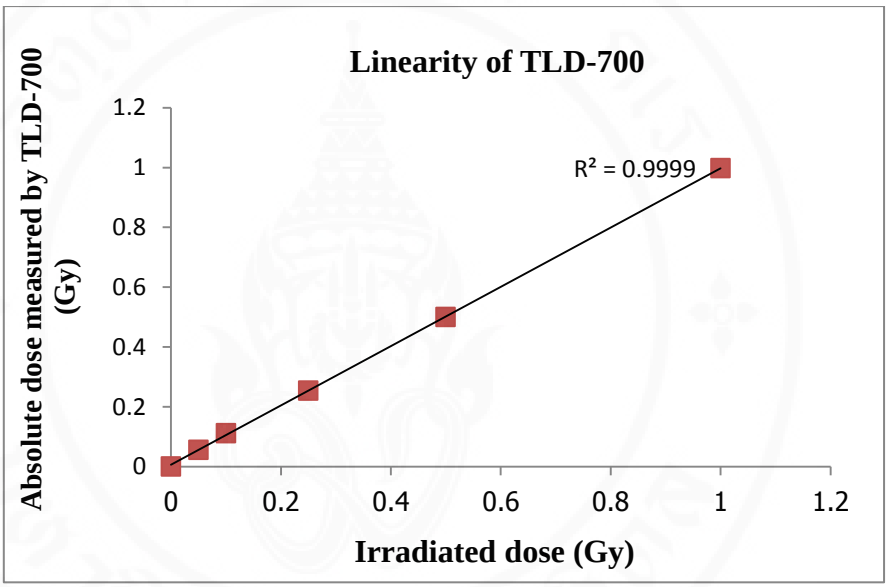

Figure A.1 The linearity of TLD-700.

2. TLD-100H preparation

2.1 TLD-100H calibration

The processes of TLD-100H calibrations were:

i) Anneal 100 chips of TLD-100H with annealing program at 240 ^{o}C for 10 minutes to eliminate the residual signal in the TLDs.

ii) TLDs were placed in a perspex phantom and irradiated by the cobalt-60 machine to achieve a dose of 0.1 Gy. The exposed TLDs were heated with preheating program at 145 ^{o}C for 10 seconds to eliminate off-peak noise before reading signal by the TLD reader.

iii) Determine the element correction coefficient (ECC_i) for each TLD by using the previously mentioned equation 11, and select 10 of all TLDs which had the ECC_i value closest to 1 used for the TLD calibrations.

iv) Measured the exposure in air with a 6 cc ionization chamber and Accu-Pro^{TM} Radcal (model 9660A) by using 120 kV, 10 mAs (100 mA, 100 ms), then converted to absorbed dose (D_w) by equation below.

$$D_w = M \times N_K \times B_w \times [(\bar{\mu}_{en}/\rho)^w_{air}]_{air} \quad (16)$$

Where M is the exposure reading in mR, exposure calibration factor (N_K) was 1, backscatter factor (B_w) was 1.21 and $[(\bar{\mu}_{en}/\rho)^w_{air}]_{air}$ was 1.0297 at HVL = 5.145 mm Al.

v) The selected TLDs (10 chips) were annealed and exposed with 120 kV, 10 mAs (100 mA, 100 ms). Calculated the corrected charge integral (Q_{ci}) of these groups, and then calculated the reader calibration factor (RCF) for the whole set of TLDs with 0.487 mGy of dose.

vi) Anneal and irradiate the rest of TLDs (90 chips) with a dose of 0.487 mGy, then calculated the individual element correction coefficient (ECC_{ci}). The ECC_{ci} value for each TLD was used to determine an unknown dose (D_u) according to equation below.

$$D_u = \frac{Qi \times ECC_{ci}}{RCF}$$

Where Q_i is the individual reading of each TLD from measurement in Rando phantom.

In this study, the ECCi value of 100 chips ranged from 0.9568 to 1.0405. The reader calibration factor (RCF) for the whole set of TLDs was 167.73552 nC/mGy with the ECC_{ci} value for each TLD used to convert the reading in nC of each TLD to absorbed dose. The ECCi and ECC_{ci} value were shown in Tables A.3-A.4

Table A.3 The element correction coefficient (ECC_i) value for TLD-100H.

TLD No.	ECC_i	TLD No.	ECC_i	TLD No.	ECC_i	TLD No.	ECC_i
1	1.0364	26	1.0398	51	1.0121	76*	1.0070
2	1.0155	27	0.9912	52	0.9863	77	0.9592
3	1.0344	28	0.9856	53	1.0276	78	0.9826
4	0.9822	29	1.0093	54	0.9719	79	0.9912
5	0.9568	30	0.9881	55	1.0323	80	1.0314
6	0.9630	31	1.0324	56	1.0269	81	1.0388
7	0.9872	32	0.9657	57	1.0339	82	0.9897
8*	1.0023	33	1.0372	58	1.0387	83	1.0111
9	1.0120	34*	1.0020	59	1.0311	84	1.0083
10	0.9801	35	0.9830	60	0.9824	85	0.9875
11	0.9629	36	1.0386	61	1.0155	86	0.9891
12	1.0184	37	0.9861	62	1.0209	87*	0.9996
13	1.0124	38	0.9878	63	1.0390	88	0.9900
14	0.9878	39	1.0376	64*	0.9991	89*	1.0017
15	0.9838	40*	0.9996	65	0.9893	90	1.0099
16	1.0307	41	1.0358	66	0.9839	91	1.0286
17	0.9584	42	0.9699	67	1.0320	92	0.9873
18	0.9854	43	1.0374	68*	0.9993	93	1.0200
19*	1.0086	44	0.9697	69	1.0260	94	0.9620
20	1.0181	45	0.9616	70	1.0120	95	0.9611
21	0.9883	46	0.9714	71	1.0185	96	0.9600
22	1.0172	47	1.0307	72	1.0382	97	0.9874
23	0.9836	48	1.0204	73	0.9756	98	1.0289
24	0.9750	49	1.0198	74*	1.0019	99	0.9662
25	1.0405	50	1.0266	75	0.9618	100	0.9614

* The TLDs selected for calibration.

Table A.4 The individual element correction coefficient (ECC_{ci}) for TLD-100H.

TLD No.	ECC_{ci}	TLD No.	ECC_{ci}	TLD No.	ECC_{ci}	TLD No.	ECC_{ci}
1	1.0074	26	1.0356	51	0.9945	76*	0.9752
2	0.8921	27	0.9762	52	0.9607	77	0.9434
3	0.9425	28	0.9788	53	1.0303	78	0.9686
4	0.9851	29	1.0172	54	0.9859	79	0.9322
5	0.9205	30	1.0327	55	1.0060	80	1.0025
6	0.9777	31	1.0256	56	1.0332	81	0.9969
7	1.0288	32	0.9760	57	1.0542	82	1.0504
8*	1.0492	33	1.0172	58	1.0682	83	1.0235
9	1.0676	34*	1.0160	59	1.0508	84	1.0051
10	1.0156	35	0.9552	60	0.9809	85	1.0120
11	0.9846	36	1.0630	61	1.0099	86	0.9940
12	1.0828	37	0.9990	62	0.9908	87*	0.9853
13	1.0065	38	0.9714	63	1.0562	88	0.9903
14	1.0178	39	1.0264	64*	0.9960	89*	0.9924
15	1.0105	40*	1.0292	65	0.9668	90	1.0061
16	1.0503	41	1.0552	66	1.0001	91	1.0120
17	0.9950	42	0.9687	67	1.0148	92	0.9907
18	1.0366	43	0.9602	68*	0.9638	93	1.0064
19*	1.0356	44	0.9843	69	1.0262	94	0.9728
20	1.0534	45	0.9788	70	0.9854	95	0.9670
21	1.0042	46	0.9827	71	0.9932	96	0.9290
22	1.0184	47	1.0616	72	1.0261	97	0.9990
23	1.0228	48	0.9965	73	0.9474	98	1.0398
24	0.9944	49	1.0225	74*	0.9852	99	0.9829
25	1.0745	50	0.9741	75	0.9122	100	0.9772

* The TLDs selected for calibration.

2.2 Linearity test of TLD-100H

TLDs chips were exposed with 120 kV, 5 mAs, 10 mAs, 20 mAs, 30 mAs and 40 mAs, respectively. The readings of all TLDs from each exposure were converted into the unit of dose. Measurement the same exposure with a 6 cc ionization chamber in the same condition of exposed TLDs, and then converted to absorbed dose. The average doses obtained from TLDs were plotted as a linear function of the absorbed dose values. In this study demonstrated a linear relation with a R^2 of 0.9969 which shown in Figure A.2

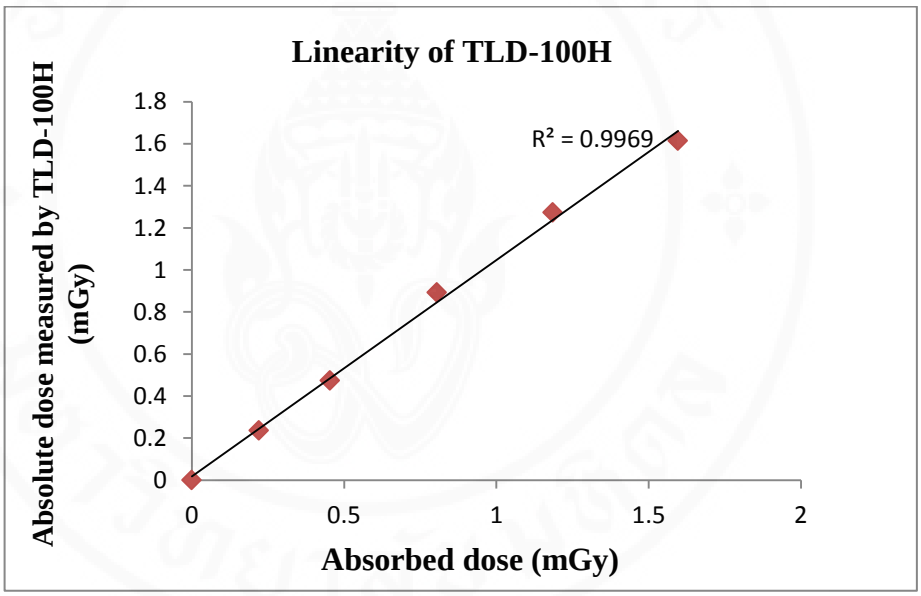

Figure A.2 The linearity of TLD-100H.

BIOGRAPHY

NAME	Miss. Rattana Watjiranon
DATE OF BIRTH	13 March 1986
PLACE OF BIRTH	Trang, Thailand
INSTITUTIONS ATTENDED	Mahidol University, 2008: Bechelor of Science (Radiological Technology) Mahidol University, 2013: Master of Science (Medical Physics)
HOME ADDRESS	48 Satonsatanpitak Road, Kantang, Trang, Thailand 92110 Tel. 075-251497